NEW ANALYSIS ON THE MECHANICS, TEMPERATURE, TOOL LIFE AND WORKHARDENING IN OBLIQUE MACHINING

by VENUVINOD K. PATRI & LAU WAI SHING

Paper presented at the Technical Conference at the 27th Anniversary of South China Institute of Technology, China on 17th Nov 1979.

Abstract

New Analysis on the Mechanics, Temperature, Tool Life and Work Hardening in Oblique Machining

by VENUVINOD K PATRI and LAU WAI SHING

The majority of cutting tools in machining have some oblique angles. Its study is therefore very important. Orthogonal cutting theory, which is in a well developed stage now, is a special case of oblique cutting and the understanding of the latter therefore would strengthen our understanding of orthogonal cutting itself.

A study of the literature in oblique cutting shows that only chip formation and mechanics have been studied to some extent. Even these are based on single slip line concept. While many other advanced techniques are available for orthogonal cutting analysis, further analysis of other important aspects like temperature, tool life, workhardening etc. have not been attempted so far. This paper gives a brief summary of the work of the authors and their associates over the last decade to fill in the above gap.

A simple and effective method have been proposed for measuring chip flow angle. A new analysis on the mechanics of oblique cutting based on the lower boundary of the shear zone using well known slip line principles has been developed. It is shown that this analysis is as effective as the single shear plane approach. Furthermore, it gives the normal pressure ahead of the cutting zone which can be predicted from orthogonal cutting using the concept of effective rake angle.

The problem of thermal analysis is attempted for the first time in the paper using oblique moving heat source. The heat sources of the shear and rake plane are resolved into lateral and normal component sources. The temperatures due to these sources are estimated using a new master chart. These are then superimposed using a specially developed superimposed formula.

..../2

Experimental data has been presented showing that the tool life and Taylor constant increase with increase in obliquity. An analysis based on adhesion wear theory has shown that the principal reason for this is the decrease in the mean temperature on the tool flank with increase in obliquity.

Experimental data is presented showing that workhardening increases with obliquity. This is attributed to additional shear along the shear zone. A method of predicting workhardening in oblique cutting based on cutting forces is presented.

New analysis on the Mechanics, Temperature, Tool Life and Work Hardening in Oblique Machining

1. INTRODUCTION

The importance of oblique cutting in the field of metal cutting needs little emphasis. Most of cutting tools have some magnitude of obliquity [i] of the cutting edge. For single point-tools (Fig 1.1a) the obliquity may range from 6 to 25°. For cylindrical milling cutters the obliquity (Fig 1.1b) may be as high as 60°. It is therefore important to know the effects of i on various metal cutting aspect like chip geometry, cutting forces, cutting temperatures, tool wear, tool life and integrity and nature of machined surface.

Historically, the study of obliquity has attracted the attention of metal cutting investigators for a long time. Merchant [1] made an analysis of the equilibrium of the chip under cutting forces in oblique cutting. This approach was examined experimentally by Shaw et al later [2]. Stabler [3] proposed the relationship that chip flow angle is equal to i. He tried to show that this follows from the considerations of minimum energy [4]. Oxley [5], Bobrov [6] etc did parallel but similar studies. The concept of effective rake angle, first proposed by Shaw et al has been a subject much controversy (Armarego and Brown, [7]). The list mentioned here gives only the land marks but by no means gives a comprehansive list. In addition, to these fundamental studies there have been a number of investigations trying to extend the results to practical cutting tools like drills [8], form tools for V-form [9] etc. There is another class of metal cutting operations like rotary cutting where the rotary speed simulates an effect similar to that of obliquity i. Studies have been done to extend the basis oblique cutting theory to these operations [10,11,12].

Most of the investigations suggested above largely confined themselves to chip geometry and cutting forces. The subjects of temperatures, tool life, and surface integrity have received lesser fundametal treatment. Further, these theories have been generally an extension of simple shear plane approaches. The study of mechanics of oblique cutting has progressed little beyond the classical shear plane approach proposed about 35 years ago. Meanwhile, the study of mechanics of metal cutting has progressed considerably. Bold new approaches like the application of slip line models [13,14], shear zone models [15,16] etc have been developed. However, generally speaking, the various orthogonal cutting theories are waiting for extension into oblique cutting.

The present authors have been working in the field over the last decade. This paper summarizes the work of the authors in the field. It tries to give a comprehensive view in oblique cutting covering various aspects. Some of the work reported here had been published elsewhere [17,18]. Others are under preparation for publication.

Since the paper tries to cover a wide range of features, the discussion of each item has,of necessity,been reduced to the minimum. Wherever possible, standard nomenclature has been used. The meanings of various terms should be evident to one who is aware of classical literature on the subject. Emphasis is placed on new concepts proposed; while taking classical concepts for granted. Again, for the sake of brevity, it has been possible to include only a few of the experimental data obtained in support of proposed concepts.

2. MEASUREMENT OF CHIP FLOW ANGLE

2.1 Introduction

The presence of chip flow angle is the chief characteristic that differentiates between the chip geometries obtained in oblique and orthogonal cutting. The importance of chip flow angle in oblique machining needs no emphasis. Almost all models of chip formation in oblique machining include it is an important parameter. Experimental estimation [19,20] or theoretically predicting [21,22] the chip flow angles have been proposed and used. However, the methods reported are generally suffering from limitations of either lack of accuracy or requires tedius and expensive experimental set up. The present method describes a simple but reliable method of estimating the chip flow angle in oblique cutting.

2.2 The Method

Fig 2.1 shows schematically the geometry of chip formation in oblique cutting. Consider any arbitrary grid on the uncut surface of the workpiece inclining at an angle ψ (Fig 2.2a). Fig 2.2b is a magnified view as the grid line AB approaches the cutting edge.

$CB = b \tan \psi$

$CD = b \tan i$

$BD = CD - CB = b(\tan i - \tan \psi)$

Time for B to travel to D $= \frac{BD}{V}$

At the same time A will travel to E, time required $= \frac{AE}{V_c}$

$$\frac{b(\tan i - \tan \psi)}{V} = \frac{AE}{V_c}$$

$$AE = \frac{V_c}{V} b(\tan i - \tan \psi)$$

$$= \frac{1}{r_c} b(\tan i - \tan \psi)$$

From geometry,

$$\frac{AE}{\text{Sin}\lambda} = \frac{AD}{\text{Sin}\ (180 - \theta)}$$

$$\therefore \quad \frac{1}{r_c} \quad \frac{b(\tan i - \tan\psi)}{\text{Sin}\ \lambda} = \frac{\frac{b}{\text{Cos}\ i}}{\text{Sin}\ \theta}$$

$$\therefore \quad \lambda = \text{Sin}^{-1}\left[\frac{1}{r_c}\ \text{Cos}\ i\ (\tan i - \tan\psi)\ \text{Sin}\ \theta\right]$$

and $$= 90^{o} - \theta + \lambda$$

$$= 90^{o} - \theta + \text{Sin}^{-1}\left[\frac{1}{r_c}\ \text{Cos}\ i\ \text{Sin}\ \theta\ (\tan i - \tan\psi)\right] \qquad (2.1)$$

Two cases of formula (1) are of interest,

(i) when $\psi = 0$; $$= 90^{o} - \theta + \text{Sin}^{-1}\left[\frac{1}{r_c}\ \text{Sin}\ i\ \text{Sin}\ \theta\right] \qquad (2.2)$$

(ii) when $\psi = i$; $$= 90^{o} - \theta \qquad (2.3)$$

Use of case (1) requires scribing a line initially on the unmachined surface in a direction prependicular to the cutting velocity. It requires two measurements, that of r_c and θ.

Use of case (ii) requires scribing a line initially on the unmachined surface in the direction of the cutting edge. It requires only one measurement, that of θ.

2.3 Measurement of θ

A line can be scribed on the unmachined surface in the direct of the cutting edge. After the cutting test has been performed, the chips are collected and their lengths measured. The angle θ is the angle between the direction of chip flow and the direction of the scribed line after deformation. The chip flow direction can be measured from the scratch marks of the previous cut and the scribed lines on the chip surface, the angle between the scratch mark and the scribed line then gives the value of θ and from formula (2.3), $\rho = 90^{o} - \theta$.

2.4 Observation

From the data obtained, the chip flow angle was estimated by the present method, and other methods from the formula given in the Introduction. All comparisons have been made taking the results obtained from photographic method as the standard.

Fig 2.3 shows the comparison of ρ obtained from various methods to that obtained by photographs. It shows that the chip flow angles obtained from formula (2.1) agree very strongly with that from photographs.

The chip flow angles calculated from both the force methods give poor correlation. The chip width method by far is the worst method and leads to inadmissible values at low angles of inclination owing to side spread.

Fig 2.4 shows the correlation between ρ obtained from formula (2.2) to that of formula (2.3). The almost one to one correspondence indicates that both formulae are equally accurate.

Fig 2.5 & 2.7 are some instant observations using data obtained by formula (2.2).

Fig 2.5 & 2.6 show the effect of depth of cut on chip flow angle. It can be seen that for small depth of cuts, Stabler's rule is obeyed. However, as depth of cut increases, ρ is found to increase.

Fig 2.6 shows that the velocity of cut does not have any effect on chip flow angle.

Fig 2.7 shows the deviation of ρ obtained from various methods from Stabler's rule. From the experiment, it can be seen that Stabler's rule applies only to very small inclination angles and small depth of cut.

3. MECHANICS OF OBLIQUE CUTTING USING A PSEUDO-SLIP LINE

Today, there exist a variety of models for orthogonal cutting. These cover a wide range of concepts with the simple shear plane models at one end and the complex slip line models at the other end. Each model emphasises a particular aspect at the cost of others. Yet, it is the existance of this variety which enables us to have an understanding of the totality of metal cutting though no single model is able to cover the totality.

The situation with oblique cutting is entirely different. With the exception of shear plane models [1] and others involving mean shear zone thickness [6] etc., no serious attempt has been made to extend other models of orthogonal cutting to problems of non-plane-strain cutting. Such extensions are, however, desirable since they would throw more light on aspects hitherto unexplored in oblique cutting. This will also test the model in a new environment and would throw greater light on its advantages and limitations.

This paper aims at extending to oblique cutting, a pseudo-slip line solution proposed by Connally and Rubenstein [23] for orthogonal cutting. After developing the model it is verified against the experimental data available in literature and the implications discussed.

3.1 Connally and Rubenstein's Orthogonal Cutting Model

Fig 3.1a shows the assumed bounds of the primary deformation zones. These bounds must obviously be slip lines. Consider a slip line close to the lower bound. For simplicity, let the transient curve joining the unmachined surface to the chip surface be ignored. The slip line then meets the unmachined surface at 45 deg. OB is then the nominal shear plane used in Merchant's [24] analysis. The slip line is further assumed to be parallel to the cutting speed at the end it meets the cutting edge. This feature and the absence of the transient surface are valid flaws in the model.

The cutting forces contributed by chip formation can be estimated if the stress distribution on the slip surface are known.

It is more attractive to consider a slip surface close to the lower boundary of shear zone, since the material there is still in the virgin state. The curvature of the lower bound surface is usually low. It is therefore permissible to replace the slip surface by two planes (S and L-planes) parallel to it at each end. The error involved in such a procedure would be low as far as the estimation of cutting forces is concerned. It would of course be undersirable to stretch the model to other aspects of machining like the determination of exact stress and strain distributions etc.

The stress distribution along the S and L planes may be estimated from the well known properties of slip lines. Integrating these stresses and taking appropriate components it is possible to estimate the cutting forces. Such estimations made by Connally and Rubenstein [23] agreed well with experimental observations. The length 'l' of the L-plane is taken as a parameter similar in scope to the shear angle in conventional analysis.

3.2 The New Oblique Cutting Model

On the basis of empirical evidence, it may be said that the primary effect of obliquity is to change the orientation of slip on the slip surfaces on the primary deformation zone. When one attempts at the extension of Connally and Rubenstein's model to oblique cutting, one is tempted to keep the S and L-planes as they are and introduce lateral slips. This is in line with Merchant's [1] approach where he introduced lateral slips on the conventional shear plane to take into account the effect of obliquity. However, this would mean that the actual slip lines are now inclined to the normal plane. If the S plane is kept inclined to the cutting

plane at 45 deg, the slip lines would meet the free surface at an angle less than 45 deg. It is therefore necessary to change the orientation of S-plane accordingly.

Fig (3.1b) illustrates the basic features of the proposed model. RS is the cutting edge. Plane RJKS is the nominal shear plane. Curved surface RJKS is the slip surface under consideration. Planes PJKQ (S-plane) and PQSR (L-plane) are drawn tangential to surface RJKS at each end. The S-plane is inclined to the cutting plane at angle ψ_η whereas the L-plane is in it. PQ is the line of intersection of the S and L-planes. l_η is the length of S-plane.

Shear is assumed to take place on surface RJKS in the direction represented by curve OB. For simplicity it is assumed that OB is a plane curve perpendicular to the cutting plane. θ is the angle made by this characteristic plane with the normal plane. θ may thus be considered as the lateral shear angle in the L-plane. ψ_ℓ is the corresponding angle in the S-plane. AB which is tangential to the orientation of shear in the S-plane should be at 45 deg to the cutting plane. From the geometry of Fig (3.1b) the following expressions can now be obtained.

$$\tan \psi_\eta = \sec \theta \text{ or } \operatorname{cosec} \psi_\eta = (1 + \cos^2\theta)^{\frac{1}{2}} \qquad (3.1)$$

$$\sin \psi_\ell = \sin \theta / \sqrt{2} \qquad (3.2)$$

and

$$l_\eta = a (\cos \phi_\eta - \cos \theta) \qquad (3.3)$$

Where $$\phi_\eta = \frac{\cos \alpha_\eta}{a_c/a - \sin \alpha_\eta} \qquad (3.4)$$

The areas A_s and A_L of the S and L-planes are given by

$$A_s = aw (1 + \cos^2 \theta)^{\frac{1}{2}} \qquad (3.5)$$

and

$$A_L = aw (\cot \phi_\eta - \cos \theta) \qquad (3.6)$$

It may be noticed that angle $\psi_\eta \geq 45$ deg. For orthogonal cutting $\theta = 0$, $\psi_\eta = 45$ deg as assumed in the orthogonal cutting model. As in the case of orthogonal cutting ι_η may be interpreted as a parameter similar in scope to the shear angle but in the present case it also includes the effect of obliquity indirectly through θ.

The S-plane extends upto the free surface. Therefore the normal and shear stresses on the plane are equal to the flow stress τ_s of the work material. Multiplying these stresses with the area A_s of the plane the magnitudes of the shear force S_s and normal force N_s can be found. From the knowledge of angles ψ_η and ψ_1 these forces can be divided into the normal (S_{sn}, N_{sn}). Lateral (S_{s1}) and thrust (S_{sy}, N_{sy}) components. Plane L being a slip plane, the shear stresses on it is again τ_s. But the mean normal stress 'P' on it is unknown. Multiplying these stresses with the area A_L of the plane, the shear (S_L) and normal forces (N_L) can be determined. These can be resolved further into the normal (S_{Ln}), lateral (S_{L1}) and thrust (N_L) components. Cutting force components P_n', P_ℓ' and P_y' may be obtained by summing up the appropriate components from the above.

The following expressions are obtained after simplification.

$$P_n' = S_{sn} + N_{sn} + S_{Ln}$$

$$= \tau_s A_s \cos 45 \text{ deg} \cos\theta + \tau_s A_s \sin\psi_n + \tau_s A_L \cos\theta$$

$$= \tau_s aw \left[1 + \cos\theta \left(\frac{1 + \cos^2\theta}{2}\right)^{\frac{1}{2}} - \cos\theta + \cos\phi n\right] \qquad (3.7)$$

$$P_1' = S_{S1} + S_{L1}$$

$$= \tau_s A_s \cos 45 \text{ deg} \sin\theta + \tau_s A_L \sin\theta$$

$$= \tau_s aw \sin\theta \left(\frac{1 + \cos^2\theta}{2}\right)^{\frac{1}{2}} - \cos\theta + \cot\phi_n \qquad (3.8)$$

$$P_y' = S_{Sy} + N_{Sy} + N_L$$

$$= \tau_s A_s \sin 45 \text{ deg} + \tau_s A_s \cos\psi_n + p A_L$$

$$= aw \left[p (\cot\phi_n - \cos\theta) - \tau_s \cos\theta - \tau_s \left(\frac{1 + \cos^2\theta}{2}\right)^{\frac{1}{2}}\right] \qquad (3.9)$$

An expression for parameter θ may be obtained by dividing equation 7 with equation S. Thus, in terms of force components P_n' and P_1' we have,

$$\cos\theta - \left(\frac{P_n'}{P_1'}\right)\sin\theta + \left[\frac{1+\cos^2\theta}{2}^{\frac{1}{2}} - \cos\theta + \cot\phi_n\right]^{-1} = 0 \qquad (3.10)$$

It will be shown later through empirical evidence that $\theta \simeq i$. Substituting this equality in equation 3.7 one has

$$P_n' = \tau_s\, aw \left[1 + \cos i\left(\frac{1+\cos^2 i}{2}\right)^{\frac{1}{2}} - \cos i + \cot\phi_n\right] \qquad (3.11)$$

It will be seen that equation 3.11 is as reliable as the more accurate equation 3.7 in predicting the normal force P_n'. However, when the substitution $\theta \simeq i$ was incorporated into equation 3.8 and checked with experimental data the errors were found to be too high.

3.3 Application of the Model to Experimental Data and Discussion

With a view to testing the validity of the assumptions made and the accuracy of the equations developed in the above analysis, the model has to be tested on a wide variety of published experimental data. However, only a few typical results are discussed below.

Consistency of the value of dynamic flow stress 'S' for a given workpiece material is taken as the test criterion in the following. In eqn. (3.7) and (3.11), if one plots the coefficient of 'S' against the force component, F_n, if the magnitude of 'S' is constant and the 'tool edge' and 'flank' conditions have not changed drastically, one may expect all the data points to fall approximately on a straight line. The slope of the straight line would then give the magnitude of 'S' and the intercept on the F_n axis would represent the contribution due to the cutting edge radius and the tool flank. Figs. 3.2 to 3.4 show such straight lines obtained from the data obtained from references 25,26, and 27 respectively.

In all the three cases it is observed that the data points are close to the straight lines drawn. The magnitude of 'S' in each case is reasonable for partially work-hardened workpiece material. Among themselves, figs 3.2 to 3.4 cover a wide range of cutting speed (2.5 - 746 ft/min) normal rake angle (-10 to 36^{o}), inclination angle ($0-60^{o}$) and uncut chip thickness (0.002-0.012"). This establishes the validity of the model in a wide range of cutting conditions and tool geometry.

The shear force on Merchant's shear plane is given by

$$F_s = \left[\left[F_n \cos \phi_n - F_z \sin \phi_n \right]^2 + F_t^2 \right]^{\frac{1}{2}}$$

To estimate the magnitude of shear stress S* on Merchant's shear plane (given by $Wt_1/\sin \phi_n$), and obtain the slope of the resulting straight line. Figs. 3.5 to 3.7 show such plots obtained from data given in references 25,26,27 respectively. Comparing these with figs. 3.2 to 3.4 it is observed that the scatter in figs 3.2 to 3.4 is of the same order as that in figs. 3.5 to 3.7. It is also noted that the magnitude of S is normally less than S*, but not as small as to be equal to the flow stress of the non-work-hardened workpiece material. This indicates that the slip-line analysed is not exactly the lower boundary of the primary deformation zone but lies somewhere in the region between the lower boundary and Merchant's shear plane.

....12

Figs 3.8 to 3.10 show the variation of θ with varying i, from the data obtained from references 25,26 and 27. It can be observed that :

(i) θ is always less than i.

(ii) The difference $(i-\theta)$ increases as i increases.

(iii) $(i-\theta)$ is of the order of 7 to 10^{o} even at inclination angle as high as 50^{o}.

3.4 The normal pressure on the L_n plane

The normal pressure p, on the L_n plane in oblique cutting can be solved once θ and S are knwon,

i.e. $$F_z = WS \frac{t}{\sin \theta} \left\{ \cos 45^{o} - \cos \theta \right\} \sec i$$

$$+ P_1 \, Wt \, (\cot \phi_n - \cot \psi_n) \sec i$$

From orthogonal cutting using rake angles equal to the effective angles in oblique cutting, the normal pressure on L plane P_1 can be obtained by the equation $P_1 = \frac{F_v}{WL}$

Fig 3.8 shows that the normal pressures in both cases are identical. It is thus possible to predict the normal pressure of oblique cutting using orthogonal cutting data. This is one aspect of how effective rake angles can be used. The application of the normal pressure will be shown later.

4. WORK HARDENING IN OBLIQUE CUTTING

In earlier publications [28,29], it has been shown that the workhardening produced by orthogonal cutting is in fact caused by:

(i) Tensile stress ahead of the tool.

(ii) Burnishing effect due to the cutting edge radius and the flank.

When a metal is subjected to a strain above its elastic limit, work hardening will occur. The work hardened metal will not return to its original hardness even if the strain is completely released. This induced hardness will only disappear by a re-crystallization process. If a strain is again applied to this work hardened material, a further work hardening will take place. Assuming a linear relationship between the work hardening and the strain applied, the total work harding produced will be the sum of the work hardenings produced by the two strains applied respectively. It is thus reasonable to assume that work hardening can be additive,

viz: $hm = ha + ho + hs$

where hm = total hardness

ha = bulk hardness of material

ho = hardness caused by burniship

hs = hardness due to tensile stress ahead of tool.

In oblique machining, the above relationship can be extended to include the effect of obliquity. Thus $hm = ha + ho + hs + hT$ (4.1)

Where hT = hardness due to lateral shear.

ho is obtained from hm V_s t_1 at t = 0 at various i's Fig (4.1) shows an experimental relationship between ho and the vertical cutting edge component. It can be ssen that ho $\doteqdot$ 0.3 Fv' for aluminium alloy. From section (3.4) it has been experimentally proved that the mean normal pressure P_1 for oblique cutting is identical to that for orthogonal cutting with $\alpha = \alpha_e$.

Since in orthogonal cutting, hs $\propto$ $t_2 \sec \alpha_e$,

for aluminium alloy, $hs = 5.2 \times 10^3 \; t_2 \sec \alpha_e$.

Therefore: $hm = ha + 0.3 \; Fv' + 5.2 \times 10^3 \; t_2 \sec \alpha_e + hT$

Fig (4.2) shows that the total surface hardness ht increases linearly with increasing depth of cut. Furthermore, the hardness increases with increasing inclination angle which agrees with formula (4.1). The intercept on the hm axis gives the values ho at different i.

Once ha, ho are known and hs obtained from the orthogonal cutting data, hT can be obtained, viz

$$hT = hm - ha - ho - hs$$

Fig (4.3) shows the relationship between hT and Fx' , the horizontal cutting edge force component along the cutting edge. It is seen that $hT \propto Fx'$ and the constant of proportionality depends on the work hardening characteristic of the material. Fig (4.3) gives an equation of

$$hT = 0.08\ Fx'$$

Thus the work hardening of oblique machining of aluminium alloy can be predicted by the following equation:

$$hm = ha + 0.3\ Fv' + \left[5.2 \times 10^{3} t_2 \sec \alpha\right]_{\alpha=\alpha_e} + 0.08\ Fx'$$

Similar equations can be developed for other materials. Once the equations are developed, the work hardening can be predicted by cutting force data.

5. THERMAL ANALYSIS OF OBLIQUE CUTTING

The theory of moving heat soruces, as developed by Carslaw and Jaeger [30,31] has been widely used for the thermal analysis of orthogonal cutting [27,28,29]. 25 years back, no theory is yet available for oblique cutting. Some work undertaken recently under the supervision of the authors [35] has successfully extended the orthogonal theory to oblique cutting. This involved developing a new equation which enables the superposition of two orthogonally moving heat sources. The development of this principle and its application to oblique cutting are now briefly summarized.

5.1 Carslaw and Jaeger's Moving Heat Source Theory

Fig 5.1 shows a rectangular friction heat source of size (2ℓ x $2m$) moving on a semi-infinite conducting solid at velocity V normal to the source base ($2m$). The friction force is F so that the source strength

$$q = \frac{FV}{4\ell mJ} \tag{5.1}$$

Based on the work of Carslaw and Jaeger [25] it is possible to express the mean temperature rise $\Delta\bar{\theta}$ as

$$\Delta\bar{\theta} = \frac{q\ \alpha\ \bar{G}}{KV(2\pi)^{\frac{1}{2}}} \tag{5.2}$$

Carslaw and Jaeger [25] have shown that for (i) circular sources when $L = \frac{V\ell}{2\alpha} > 1$ and (ii) for rectangular sources when aspect ratio $AR = \frac{m}{\ell} > 2$ and $L > 0.2$ we have

$$\bar{G} = 3.8\sqrt{L} \quad \text{so that} \tag{5.3}$$

$$\Delta\bar{\theta} = \frac{C_1\ q}{\sqrt{V}} \tag{5.4}$$

$$\text{where } C_1 = \frac{1.9}{K}\sqrt{\frac{\ell\alpha}{\pi}} \tag{5.5}$$

C_1 is thus a constant for given ℓ, α and K.

5.2 Superposition Rule for Obliquely Moving Sources

Fig (5.2) shows the same source moving obliquely at angle β to the normal line ON. The velocity V can be resolved into components

$$V_n = V\cos\beta \text{ and } V_\ell = V\sin\beta \tag{5.6}$$

The friction force can likewise be resolved into components

$$F_n = F\cos\beta \text{ and } F_\ell = F\sin\beta \tag{5.7}$$

The sources may now be imagined to be the result of superposition of two orthogonal sources of strengths.

$$q_n = F_n V_n = FV\cos^2\beta = q\cos^2\beta \tag{5.8}$$

$$q_\ell = F_\ell V_\ell = FV\sin^2\beta = q\sin^2\beta \tag{5.9}$$

$$\text{It is easy to see that } q = q_n + q_\ell \tag{5.10}$$

Let $\Delta\bar{\theta}_n$ and $\Delta\bar{\theta}_\ell$ be mean temperature rises due to the normal and lateral component sources. These need to be superimposed in a suitable manner to obtain the temperature rise $\Delta\bar{\theta}$ due to the original source. For simplicity, let it be assumed that the superposition rule is independent of V and the source shape (further work is continuing to verify this rigorously). An idea of the superposition-rule can now be obtained by considering a circular source so that equation (5.4) is applicable (see Fig 5.3). For such a source the aspect ratio does not change with β so that C_1 can be taken as constant. The following equations can now be easily written.

$$\Delta\bar{\theta}_n = \frac{C_1 q_n}{\sqrt{V_n}} = \Delta\bar{\theta}\,(\cos\beta)^{\frac{3}{2}} \qquad (5.11)$$

$$\Delta\bar{\theta}_\ell = \frac{C_1 q_\ell}{\sqrt{V_\ell}} = \Delta\bar{\theta}\,(\sin\beta)^{\frac{3}{2}} \qquad (5.12)$$

Combining equations 5.11 and 5.12, we have

$$\Delta\bar{\theta} = (\Delta\bar{\theta}_n^{4/3} + \Delta\bar{\theta}_\ell^{4/3})^{3/4} \qquad (5.13)$$

Thus it is possible to assess $\Delta\bar{\theta}_n$ and $\Delta\bar{\theta}_\ell$ and superimpose them to obtain $\Delta\bar{\theta}$. The effect of source shape and velocity can still be included in the invidual estimation of $\Delta\bar{\theta}_n$ and $\Delta\bar{\theta}_\ell$. It may be noted that if the normal source is 'wide' ie. $m/\ell>1$ then automatically the lateral source is 'narrow' ie $m/\ell<1$. But equation (5.4) is applicable only when $m/\ell>1$ and $L>0.2$. It is therefore necessary to know the values of G for the values of m/ℓ and L. This has been recently done [6] by drawing a special computer programme drawn using the basic partial differential equations [30, 31]. Fig 5.4 shows the resulting nomogram.

The theory of obliquely moving heat sources is necessary in oblique cutting analysis because the source velocities (V_s and V_c) involved in this case are not perpendicular to the source bases i.e. the cutting edge.

5.3 Estimation of shear plane temperature in oblique cutting

The area of the shear plane temperature is given by

$$A_s = \frac{ab}{\cos i \sin\phi_n} \tag{5.14}$$

The velocity of shear on this plane may be resolved into normal and lateral components V_{sn} and $V_{s\ell}$ given by:

$$V_{sn} = \frac{V \cos i \cos\alpha_n}{\cos(\phi_n - \alpha_n)} \tag{5.15}$$

and $$V_{s\ell} = V_{sn} \tan\phi_\ell \tag{5.16}$$

Where $$\tan\phi_\ell = V_{sn}\{\tan i \cos(\phi_n - \alpha_n) - \sin\phi_n \tan\rho\}/\cos\alpha_n \tag{5.17}$$

The heat developed per unit area on the shear plane is given by:

$$s = \frac{F_s V_s}{A_s J} \tag{5.18}$$

A proportion R_1 is assumed to be flowing into the clip. Thus the heat flux into the workpiece is $(1-R_1)\, q_s$. The shear plane may therefore be considered as a rectangular heat source of size $(2\ell \times 2m)$ moving on the semi-infinite workpiece. The source obliquity β is obviously equal to ϕ_ℓ The source can thus be divided into normal and lateral components. The normal component source has the following properties:

$$\text{source size: } \ell_{sn} = \frac{a}{2 \sin\phi_n} \text{ and } m_{sn} = \frac{b}{2 \cos i} \tag{5.19, 5.20}$$

$$\text{Aspect ration } AR_{sn} : \left(\frac{m_{sn}}{\ell_{sn}}\right) = \frac{b \sin\phi_n}{a \cos i} \tag{5.21}$$

Source non-dimensional velocity: $L_{sn} = \dfrac{V_{sn}\ a}{4\alpha_1 \sin\phi_n}$ (5.22)

Source strength: $(1-R_1)q_s \cos^2 \phi_\ell$

The corresponding parameter $\bar{G}_{sn}$ may be obtained from Fig 5.4 for the given values of AR_{sn} and L_{sn}

Thus the temperature rise due to the normal component source is

$$\Delta\bar{\theta}_{sn} = \frac{(1-R_1)\ q_s \cos^2 \phi_\ell\ G_{sn}}{K_1\ (2\pi)^{\frac{1}{2}}\ V_{sn}} \quad (5.23)$$

The aspect ratio of lateral component source is given by

$$AR_{s\ell} = 1/AR_{sn} \quad (5.24)$$

The source non-dimensional velocity is given by

$$L_{s\ell} = \frac{Vs\ell\ a}{2\alpha_1 \sin\phi_n} \quad (5.25)$$

The parameter $\bar{C}_{s\ell}$ is obtained from Fig 5.4 for given $L_{s\ell}$ and $AR_{s\ell}$ Thus, the temperature rise due to the lateral component source is

$$\Delta\bar{\theta}s\ell = \frac{(1-R_1)\ q_s \sin^2 \phi_\ell\ \bar{G}s\ell}{K_1\ (2\pi)^{\frac{1}{2}}\ Vs\ell} \quad (5.26)$$

The resultant temperature rise $\bar{\theta}s$ on the shear plane is thus

$$\Delta\bar{\theta}s = (\Delta\bar{\theta}sn^{4/3} + \Delta\bar{\theta}s\ell^{4/3})^{3/4} \quad (5.27)$$

Now consider the heat flow into the chip. The rate of flow of heat into the chip is $R_1 q_s A_s$ which results in an average temperature rise of

$$\bar{\Delta\theta}_{sc} = \frac{R_1\ q_s}{\rho_1 C_1\ V \cos i \sin\phi_n} \quad (5.28)$$

The magnitude of R_1 may be obtained by equating $\bar{\theta}_s$ to $\bar{\theta}_{sc}$. Substituting the resulting valve of R_1 into equation 5.26 (or equation 5.28) the actual magnitude of $\Delta\bar{\theta}_s$ can be obtained. The mean temperature on the shear plane is then given by

$$\bar{\theta}_s = \Delta\bar{\theta}_s + \theta_o \quad (5.29)$$

Where θ_o is the ambient temperature.

5.4 Estimation of Rake Plane Temperature in Oblique Cutting

The area of chip tool contact area is given by

$$A = \frac{C_n\, b}{\cos i} \tag{5.30}$$

The velocity of sliding V_c at the rake plane can be resolved into normal and lateral components V_{cn} and $V_{c\ell}$ given by

$$V_{cn} = \frac{V \cos i \sin \phi_n}{\cos (\phi_n - \alpha_n)} \tag{5.31}$$

$$V_{c\ell} = V_{cn} \tan \tag{5.32}$$

The heat developed per unit area is given by

$$q_r = \frac{FV_c}{A_r J} = \frac{F\sqrt{V_{cn}^{\,2} + V_{c\ell}^{\,2}}}{A_r J} \tag{5.33}$$

A proportion R_2 of this is assumed to go into the chip. The chip tool contact area of size $(2C_n)$ x (b/cos i) is considered as a moving heat source with respect to the chip which is assumed to be a semi-infinite solid. This source can be resolved into two component sources of the following properties.

Normal component:

$$AR_{rn} = \frac{b}{2 \cos i\, C_n}, \quad L_{rn} = \frac{V_n\, C_n}{2\alpha_1}, \quad q_{rn} = R_2 q_r \cos^2 \tag{5.34 to 5.36}$$

$\bar{G}_{rn}$ is obtained from Fig 5.4 for given L_{rn} and AR_{rn}

Lateral component:

$$AR_{r\ell} = \frac{2C_n \cos i}{b}, \quad L_{r\ell} = \frac{V_{c\ell}\, C_n}{2\alpha_1}, \quad q_{r\ell} = R_2 q \sin^2 P \tag{5.37 to 5.39}$$

$\bar{G}_{r\ell}$ is obtained from Fig 4 for given $L_{r\ell}$ and $AR_{r\ell}$

Thus

$$\Delta\bar{\theta}_{rn} = \frac{R_2\, q_r \cos^2 \rho\, \alpha_1\, \bar{G}_{rn}}{K_1 (2\pi)^{\frac{1}{2}} V_{cn}} \tag{5.40}$$

$$\Delta\bar{\theta}_{r\ell} = \frac{R_2\, q_r \sin^2 \rho\alpha_1 \bar{G}_{r\ell}}{K_1\, (2\pi)^{\frac{1}{2}}\, V_{c\ell}} \tag{5.41}$$

and

$$\Delta\bar{\theta}_r = \left(\Delta\bar{\theta}_{rn}^{4/3} + \Delta\bar{\theta}_{rn}^{4/3} \right)^{3/4} \tag{5.42}$$

The chip tool contact area may now be viewed as a stationery heat source lying on the quarter-infinite tool material. The mean temperature rise is then given by

$$\Delta\bar{\theta}_{rt} = \frac{(1-R_2)\, q_r\, \ell}{K}\, \bar{A} \tag{5.43}$$

Where $\ell = C_n$ and $\bar{A}$ can be obtained substituting the aspect ratio

AR given by $\dfrac{b}{2 \cos i\, C_n}$ in equation

$$\bar{A} = \frac{2}{\pi} \left[\sin^{-1} AR + AR \sin^{-1} \frac{1}{AR} + \frac{1}{3} (AR)^2 + \frac{1}{3} \left(\frac{1}{AR}\right) - \frac{1}{3} \left(AR + \frac{1}{AR}\right) \sqrt{1 + AR^2} \right] \tag{5.44}$$

The magnitude of R_2 is now estimated from equation

$$\Delta\bar{\theta}_r + \bar{\theta}_s = \Delta\bar{\theta}_{rt} + \bar{\theta}_o \tag{5.45}$$

The resulting R_2 is substituted in equation (5.42) and the mean rake temperature $\bar{\theta}$ is then given by

$$\bar{\theta} = \Delta\bar{\theta}_r + \bar{\theta}_s \tag{5.46}$$

Fig 5.5 shows the results of the above analysis when applied to the experimental observations on a tube turning experiment on mild steel. It is seen that up to $i = 30^o$ these is little effect of i on temperature. There is a fall of 20% in temperature when i is increased up to 60^o.

6. TOOL WEAR AND TOOL LIFE

The effect of obliquity on tool life is now examined. Wear can generally be classified into abrasion, adhesion, diffusion and oxidation wears. Of these, adhesion wear is the most predominant. The last two types occur at high cutting speeds when the cutting temperatures are high. However, even in these conditions the role of diffusion process is limited to the weakening of the junctions. The actual wear still occurs by an adhesion process i.e. forming and breaking of welded junctions at the asperities on the contacting surfaces.

Starting from the fundamental principles of adhesive wear, Rubenstein [36] has developed the following experssion for the wear rate at the tool flank in the case of free orthogonal cutting.

$$\frac{d\ell_f}{dt} = p_m \frac{k_1}{\pi} p R_o^a \gamma_o^b \theta_f^q (\cot\beta - \tan\alpha) \qquad (6.1)$$

Where ℓ_f = length of flank wear land

p_m = pressure acting on flank wear land

t = cutting time

θ_f = mean temperature at the tool flank

α = rake angle

β = clearance angle

q = Schallbroch and Schaumann index ($T\theta^q$ = const)

p, R_o, γ_o, a, b etc are constants.

Experimental evidence suggests that θ_f may be taken as proportional to the mean temperature θ_r at the tool rake. θ_r in turn may be related to cutting speed V (keeping other cutting conditions and tool variables constant) by the equation.

$$\theta_r = \text{const } V^{\varepsilon}$$

Combining the above equations and comparing with Taylor's equation

$$VT^n = C$$

It is possible to show that

$$qn\varepsilon = 1$$

$$\text{and } C \propto (\cot\beta - \tan\alpha)^{-n} \tag{6.2}$$

The above analysis ignores the effect of rake angle. More recently [37] the authors have obtained the following relationship to characterize the effect of rake angle.

$$C \propto \left[(\cot\beta - \tan\alpha)^{-n} \quad (1-m^{*}\alpha)^{-\frac{1}{\varepsilon}}\right] \tag{6.3}$$

Where m is an arbitrary chosen constant satisfying the above equation.

Equation (6.3) can now be modified as

$$C \propto \left[(\cot\beta - \tan\alpha)^{n} \quad (1-m^{*}\alpha)^{\frac{1}{\varepsilon}}\right] K \tag{6.4}$$

Where K is a constant which appears in the following equation:

$$\theta_f = K\,(H_m)^{p}\, V^{\varepsilon}\, f^{\eta}\, \ell_f^{\delta}\, W^{\gamma} \tag{6.5}$$

V = cutting velocity

f = feed rate

W = B sec i = width of cut

K = constant depending on i = f(i)

Since the value of γ in eq (6.5) is very low, we can ignore the term $(B \sec i)^{\gamma}$ and thus eq (6.4) can be re-written as

$$C \propto (\cot\beta - \tan\alpha)^{-n} \quad (1-m^{*}\alpha)^{\frac{1}{\varepsilon}} \quad F(i)^{\frac{1}{\varepsilon}} \tag{6.6}$$

With this background, we now examine the likely effect of obliquity i on Taylor constant C.

Experiments were conducted by free turning a mild steel tube (outer diameter = 50mm, tube thickness = 2mm, Brinell Hardness number 110) on a lathe. The cutting tool was high speed steel (M41). The cutting temperatures (θ_m) were measured by the tool-work natural thermocouple method. The thermocouple calibration was done by the Silver Bead Technique. Fig (6.1) shows the experimental results on θ_m obtained at V= 41.5 m/min and f = 0.1mm/rev. The progress of flank wear was monitored by stopping the cutting at regular intervals and measuring ℓ_f with a microscope. The tool life criterion was set at ℓ_o= 0.18mm. Fig (6.2) shows the Taylor plots obtained at f= 0.1mm/rev at different values of i (0 to 50^o). Fig (6.3) shows the relationship between i and C.

It is seen that cutting temperature θ_m ($\simeq \theta_r$) falls with increasing i. This is attributed to the higher shear angles and lower cutting forces with increasing i observed in the experiments. A similar fall has been analytically accounted for in the previous section by using the Obliquely Moving Heat Sources Theory.

Since the normal rake and clearance angles do not change with i, we may assume that the proportionality constant between rake and flank temperatures (θ_r and θ_f) to be insensitive to i. Thus from the adhesive wear theory developed already, it follows, that tool life and Taylor constant should increase with i. This is verified in Figs (6.2) and (6.3)

There are indeed other possible effects of i (other than through θ_r). For instance, consider the moving heat source at the tool flank. As i increases this source becomes oblique and can be resolved into lateral and normal component heat sources. Even if the rate of heat liberation (q_f) at the flank is taken as constant, the narrow lateral component is likely to lead to a higher temperature. In addition, in some cases q_f itself could be a function of i. These effects would then oppose the favourable effect caused by decreasing θ_r with increasing i.

An examination of literature shows that the effect of i on tool life T is not unique. For instance, Bobrov [38] has shown T decreases with i in free oblique cutting (whereas the authors observation are the opposite). Interestingly, Bobrov still obtains a fall in θ_m with i. The only way this can be explained is by assuming that the conditions at the flank contact become more unfavourable with increasing i. Obviously, this is an intersting field to pursue in future researches.

References

1. Merchant, M.E., Basic Mechanics of the Metal Cutting Process, J. Appl. Mech., No. 3, 66, 1944.

2. Shaw M.C., COOK, N.H. and Smith, P.A., The Mechanics of Three Dimensional Cutting Operations, Transactions of the A.S.M.E., No. 6, 1952.

3. Stabler, G.V., The Fundamental Geometry of Cutting Tools, Proc. Inst. Mech. Engrs., No. 63, 165, 1951.

4. Stabler, G.V., J. Inst. Prod Engrs, Vol. 34, P284, 1955.

5. Lin, G.C.I. and Oxley, P.L.B., Mechanics of Oblique Machining: Predicting Chip Geometry and Cutting Forces From Work Material Properties and Cutting conditions, Proc. Instn Mech. Engrs., Vil. 156, pp 813-820, 1972.

6. Bobrov, V.F., VLianie Ugla Naklona Glavnoi Rezhushei Kromki Instrumenta Na Protsess Rezaniya Metallov, Mashgiz, Moscow, 1962.

7. Brown, R.H. and Armarego, E.J.A. Oblique Machining with a Single Cutting Edge, Int J. of Machine Tool Design and Research, Vol. 4, pp 9-25, 1964.

8. Fujii et al, The Analysis of Drill Geometry for Optimum Drill Design by Computer Aided Design, J Eng. Ind., A.S.M.E., pp 647-667, 1970.

9. Armarego, E.J.A., Machining with Double Cutting Edge Tools - 1, Symmetrical Triangular Cuts, Int. J. Machine Tool Design and Research, Vol. 7, pp 23-37, 1967.

10. Venuvinod, P.K., Analysis of Rotary Cutting Tools, PhD Thesis, University of Manchester Institute of Science and Technology, May 1971.

11. Narasimha Reddy, P. and Venuvinod, P.K., New Discoveries Widen the Scope of Rotary Cutting, Proc. Int. Conf. on Production Engineering, New Delhi, Vol. I, pp 243-252, August 1977.

12. Venuvinod, P.K. and Barrow, G., Recent Progress in Machining with Rotary Tools, Fifth All India Machine Tool Design and Research Conference, Roorkee, pp 173-181, 1971.

13. Lee, E.H., and Shaffer, B.W., The Theory of Plasticity Applied to a Problem of Machining, J. Appl. Mech., Tras. of A.S.M.E., Vol. 73, pp 405-413, 1951.

14. Oxley, P.L.B., Introducing Strain-rate Dependent Work Material Properties into the Analysis of Orthogonal Cutting, Annals of the C.I.R.P., Vol XIII, pp 127-138, 1966.

15. Oxley P.L.B. and Hatton, A.P., Shear Angle Solution Based on Experimental Shear Zone and Tool-Chip Interface stress Distributions, Int. Sci. Mech. Science, Vol. 5, p 41, 1963.

16. Roth, R.N. and Oxley P.L.B., Slip-line Field Analysis for Orthogonal Machining Based upon Experimental Flow Fields, J. Mech. Engg Sci., Vol. 14, No. 2, p 85, 1972.

17. Venuvinod, P.K. and LAU W.S., on the Estimation of Chip Flow angle in Oblique Cutting, Microtechnic, No. 2, Switzerland, Feb 1977.

18. Venuvinod, P.K. and LAU W.S., A New Model of Oblique Cutting, J. Eng. for Industry, Trans. of A.S.M.E., Vol 100, pp 287-292, 1978.

19. Pal, A.K. and Koenigsberger, F., Some Aspects of the Oblique Cutting Process, Int. J. Machine Tool Design and Research, Vol. 8, pp 45-58, 1968.

20. Spaans, C., Extra Forces Near Cutting Edge and Their Implication, Int. Conf. Manf. Technology A.S.T.M.E., Dearbom, Michigan, 1967.

21. LUK, W.K., The Direction of Chip Flow in Oblique Cutting, Int. J. Prod. Res., Vol. 67, No. 10, 1972.

22. Stabler G.V., The Chip Flow Law and its Consequences, Proc. 7th Int. M.T.D.R. Conf., p 243, 1966.

23. Connally, R. and Rubenstein C., The Mechanics of Continuous Chip Formation in Orthogonal Cutting, Int. J. Machine Tool Design and Research, Vol. 8, pp 159-187, 1968.

24. Ernst, H. and Merchant, M.E., Trans Am. Soc. Metals, p 299, 1941.

25. Zorev, N.N., The Mechanics of Metal Cutting, Pergamon Press, 1966.

26. Kocecioglu, D., Force Components, Chip Geometry, and Specific Cutting Energy in Orthogonal and Oblique Machining of SAE 1015 steel, Trans. of the A.S.M.E., pp 149-157, January 1958.

27. LAU W.S., An Investigation into the Factors Affecting the Work Hardening of the Workpiece Produced by Metal Cutting, PhD Thesis, University of Manchester Institute of Science and Technology, 1971.

28. Rubenstein, C. and Haslam, D., Surface and Sub-surface Work-hardening Produced by the Planning Operation, Annals of the C.I.R.P., Vol XVIII, pp 369-381, 1970.

29. LAU, W.S. and Rubenstein, C., The Influence of Tool Geometry on the Taylor Constant, Int. J. Mach. Tool Des. Res., Vol. 18, p 59, 1978.

30. Carslaw, H.S. and Jaeger, J.C., Introduction to the Mathematical Theory of the Conduction of Heat in Solids, The Macmillan and Co. Ltd., London, 1921.

31. Jaeger J.C., Moving Sources of Heat and the Temperature at Sliding Contacts, Proc. Royal Society of New South Wales, Vol. 76, P 203, 1942.

32. Loewen, E.G. and Shaw, M.C., On the Analysis of Cutting Tool Temperatures, Trans. of the A.S.M.E., pp 217-231, February 1954.

33. Trigger, K.J. and Chao, B.T., An Analytical Evaluation of Metal Cutting Temperatures, Trans. of the A.S.M.E., Vol. 73, p 57, 1951.

34. Hahn, R.S., On the Temperatures Developed at the Shear Plane in the Metal Cutting Process, Proc. First U.S. National Congress of Applied Mechanics, pp 661-666, 1951.

35. Narasimha Reddy, P., Performance of Rotary Tools, Regonal Engineering College, Kakatiya University, Warangal, India, 1977.

36. Rubenstein, C., An Analysis of Tool Life Based on Flank-Face Wear, J. Eng. Ind., Trans. of A.S.M.E., Vol. 8, p 221, 1976.

37. LAU, W.S., Venuvinod, P.K. and Rubenstein, C. The Relation Between Tool Geometry and the Taylor Tool Life Constant, accepted for publication in the Int. J. Machine Tool Design and Research, U.K.

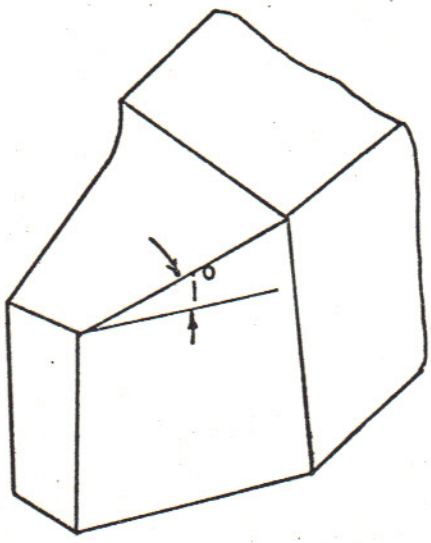

(a)

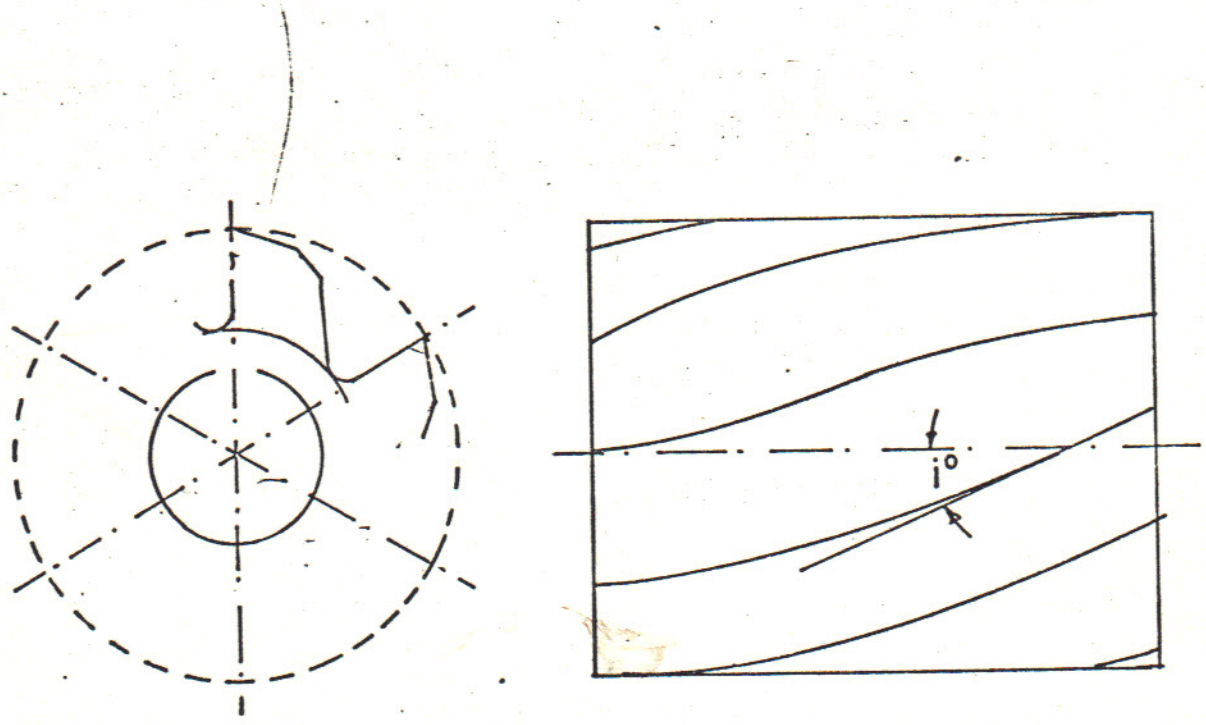

(b)

1.1 通用斜刃切削刀具

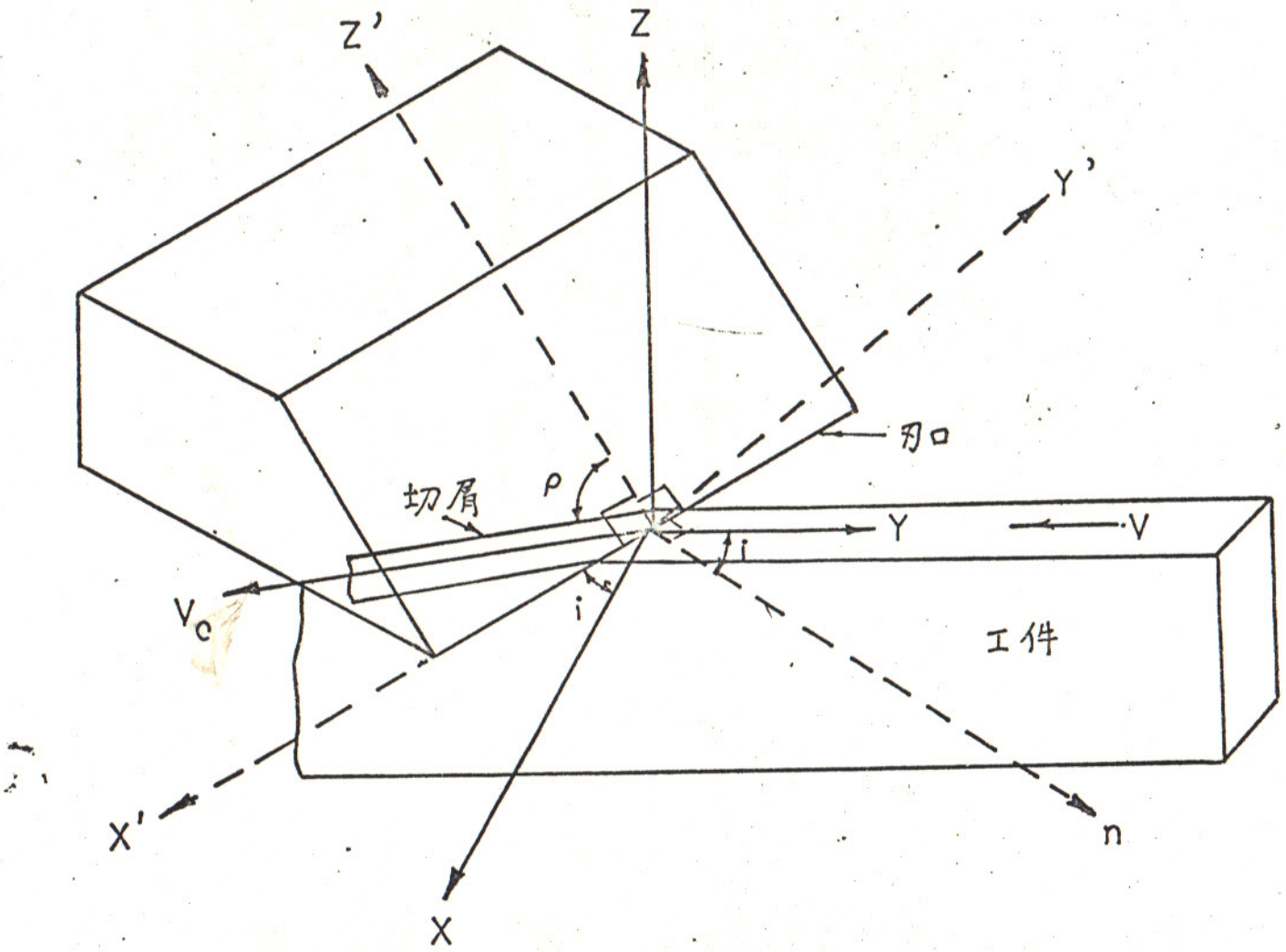

2.1 斜刃切削切屑的形成

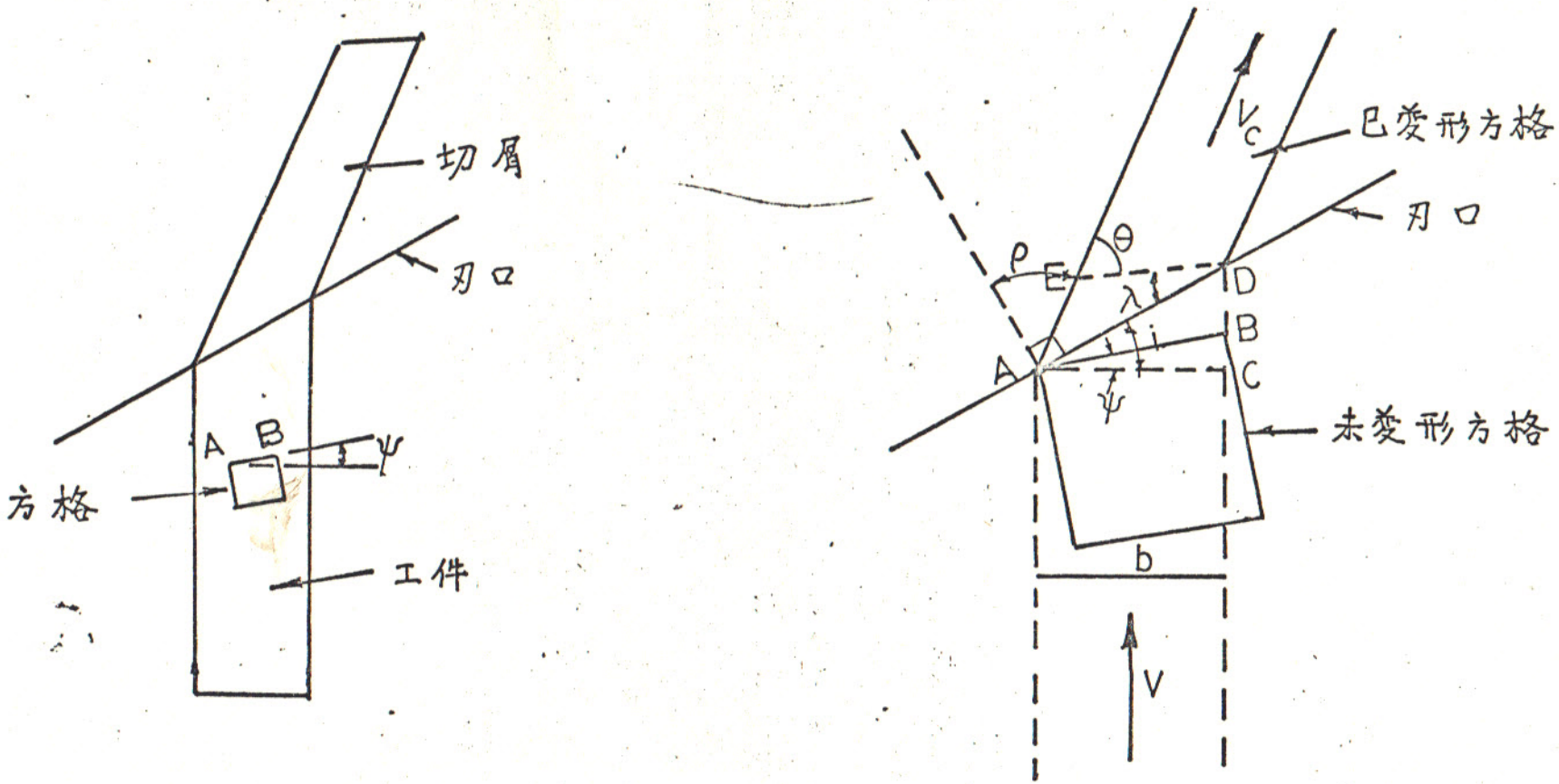

2.2 在斜刃切削時分格的動向

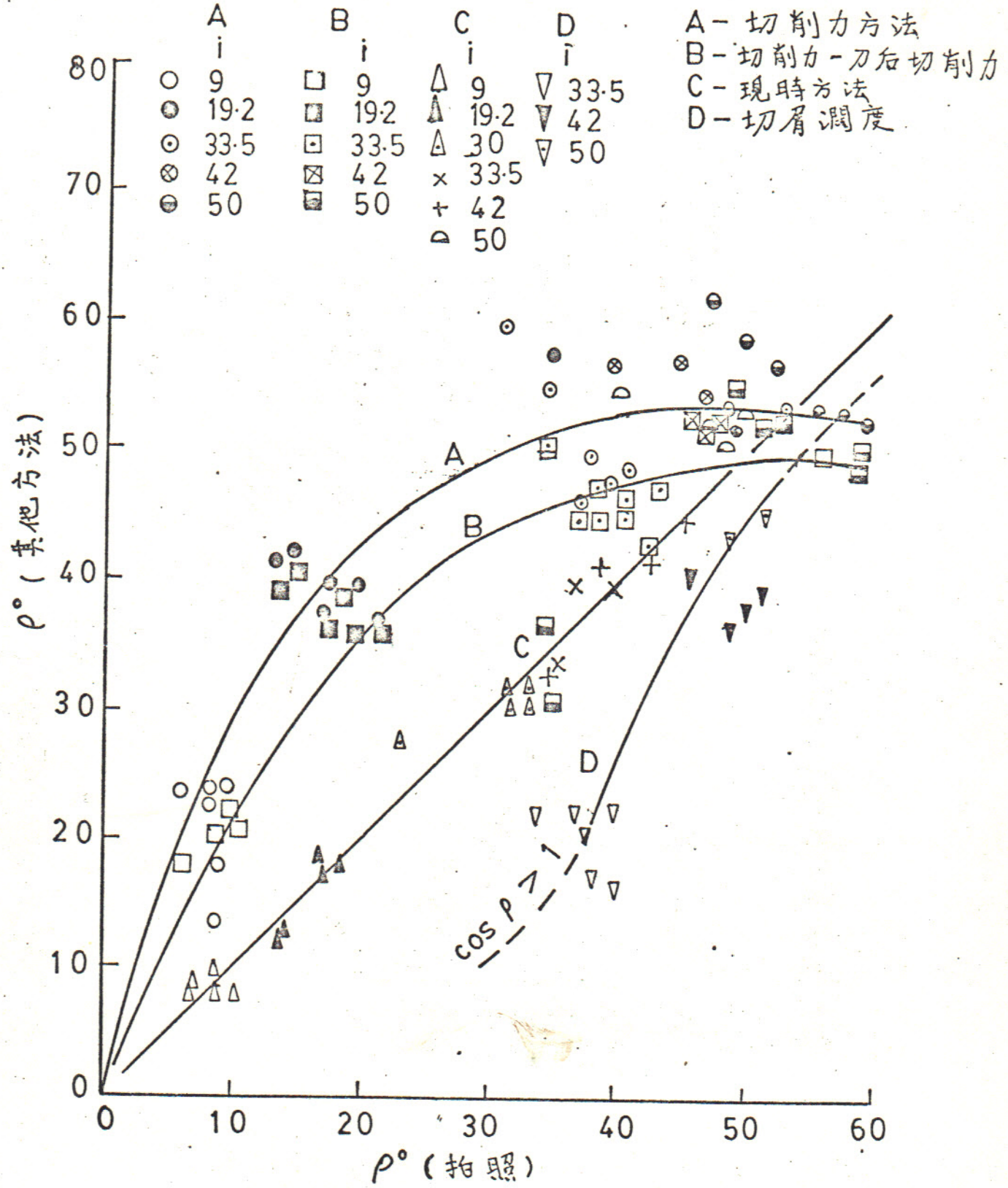

23 從不同的方法得到ρ值比較图

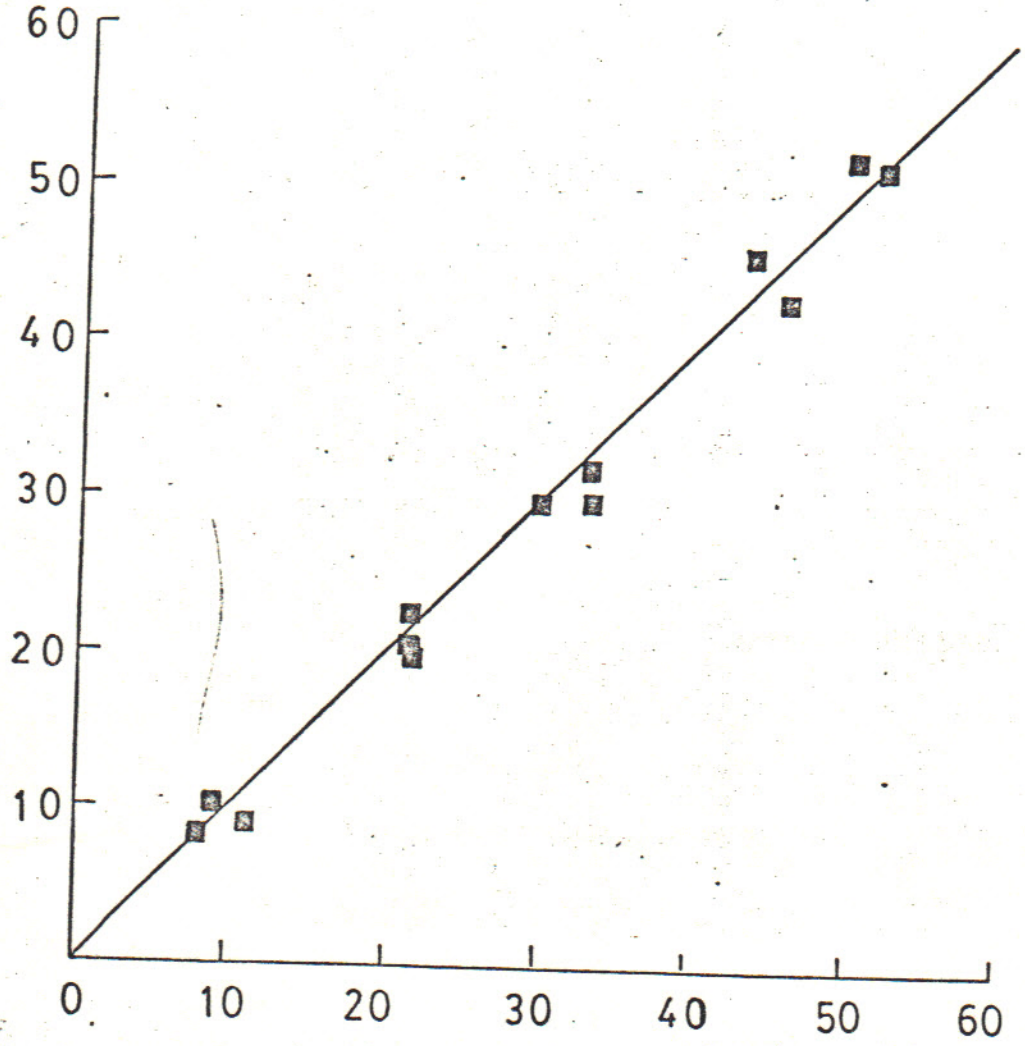

2.4 公式(2.2)及(2.3)的ρ值比較图

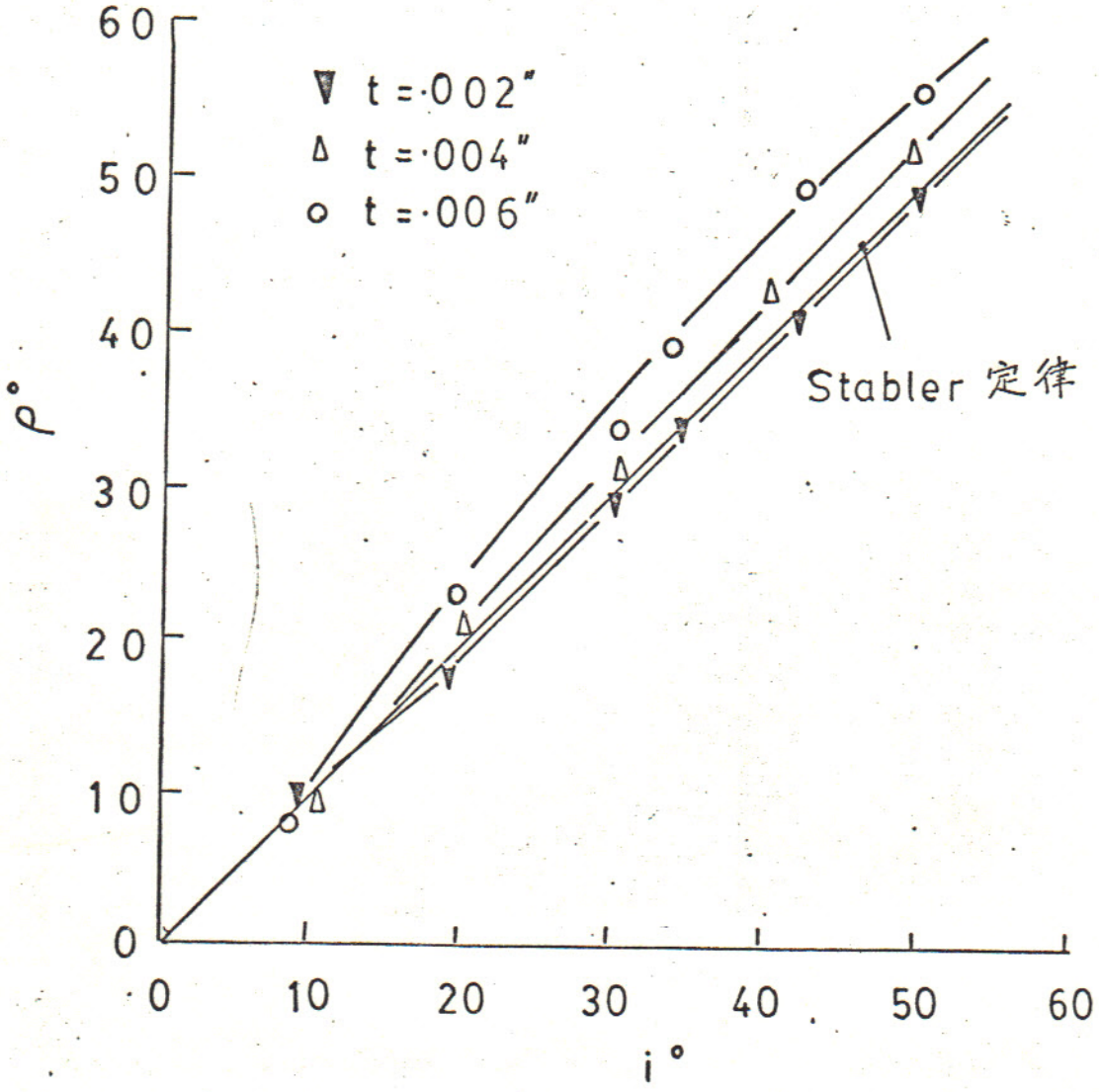

2.5 切削深度对切屑流角的影响

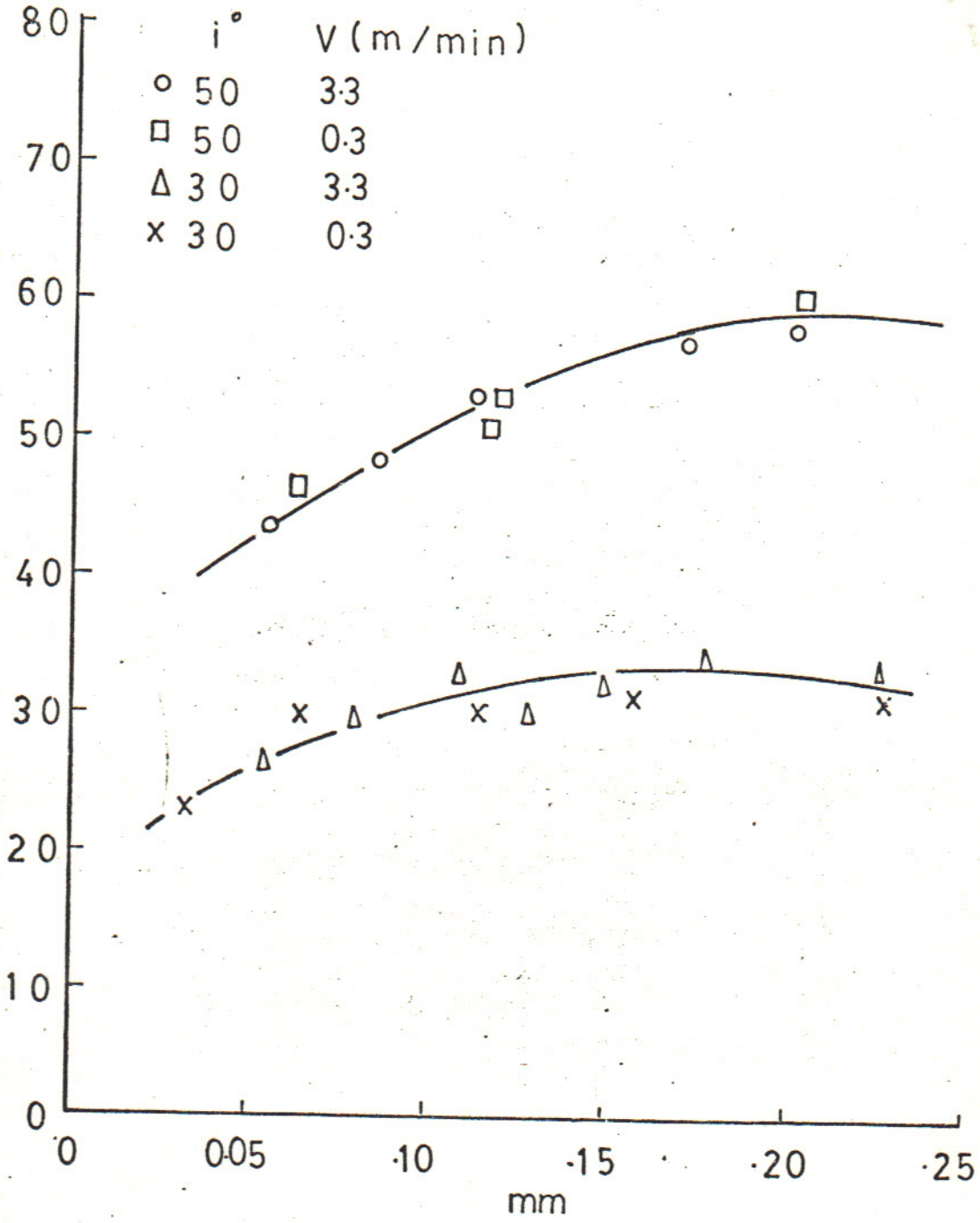

2.6 切削速度对切屑流角的影响

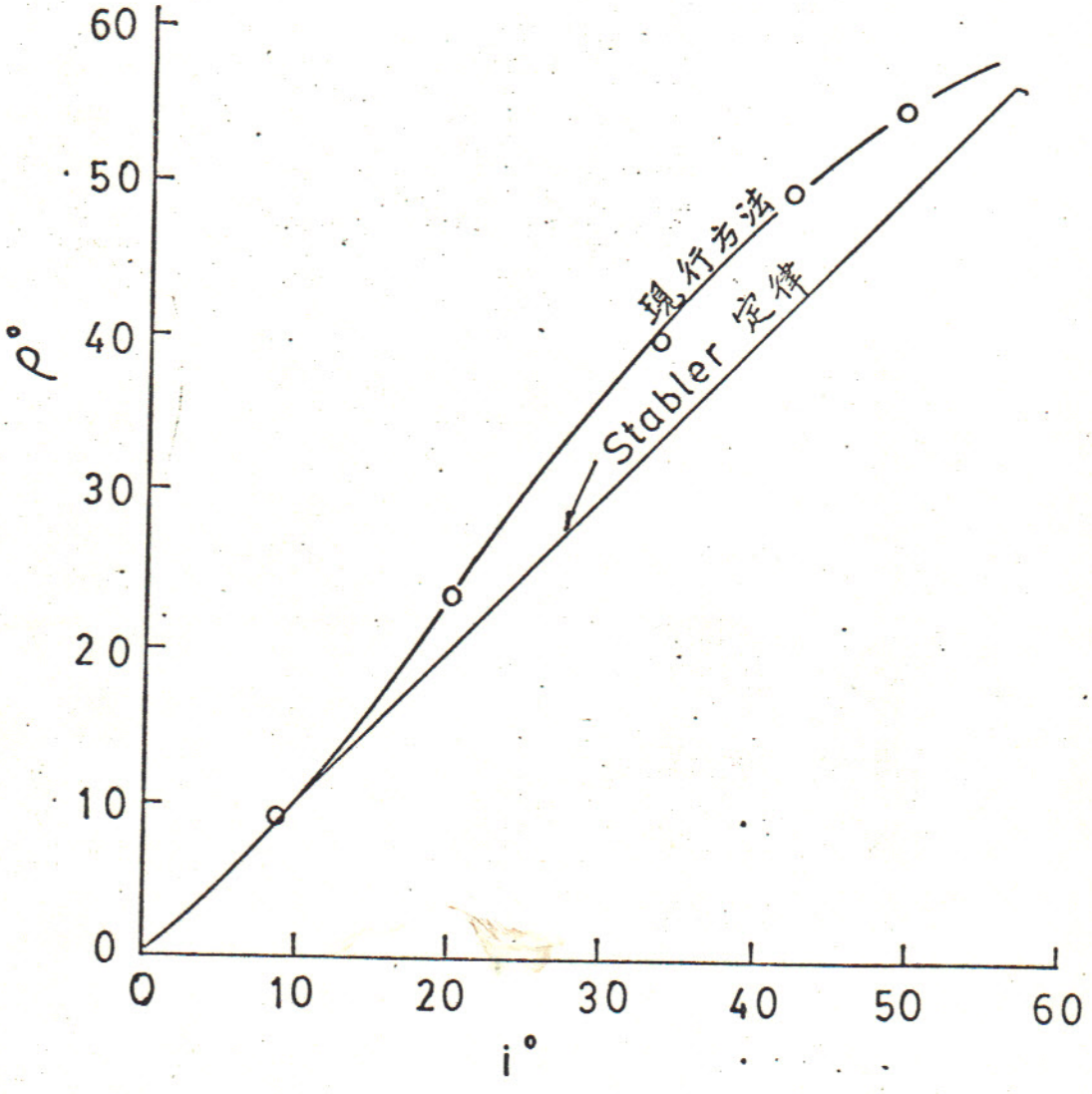

2.7 理論与 Stabler 定律的差異

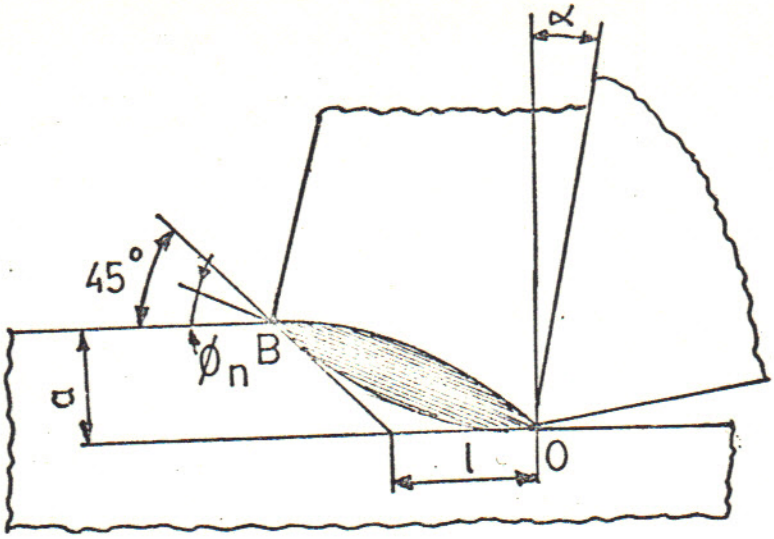
α
45°
ϕ_n
B
a
l
O

(a)

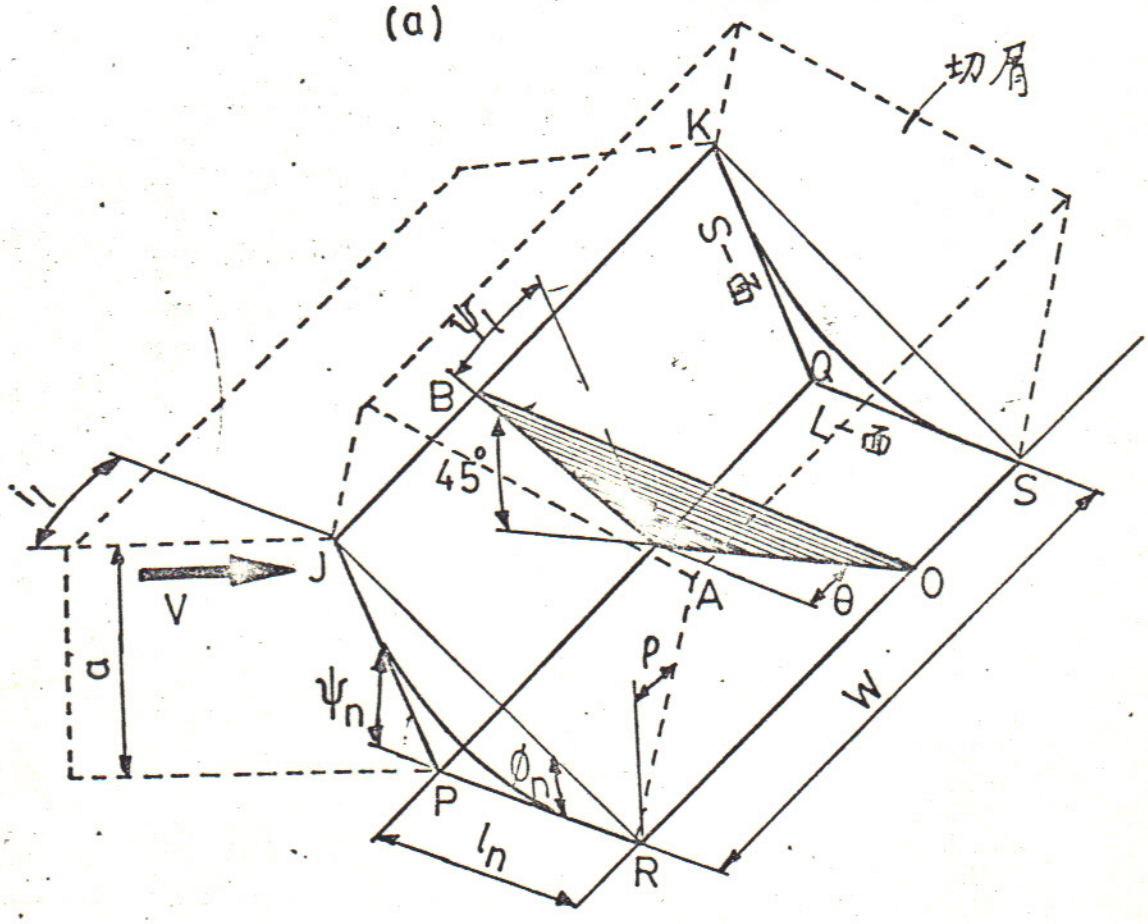
切屑
K
S面
ψ_1
B
Q
L面
45°
S
i
J
V
A
θ
O
a
ψ_n
P
W
ϕ_n
P
l_n
R

(b)

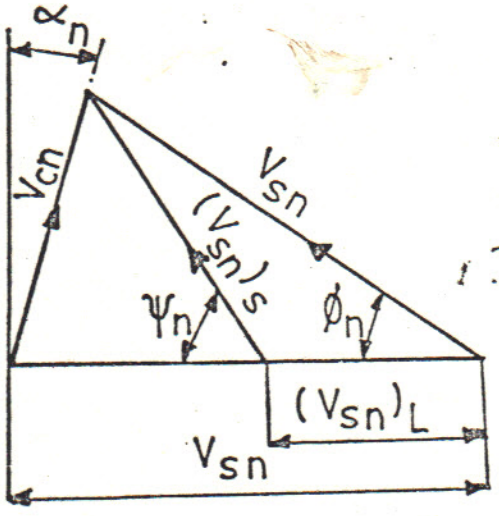
α_n
V_{cn}
V_{sn}
$(V_{sn})_s$
ψ_n
ϕ_n
$(V_{sn})_L$
V_{sn}

(c)

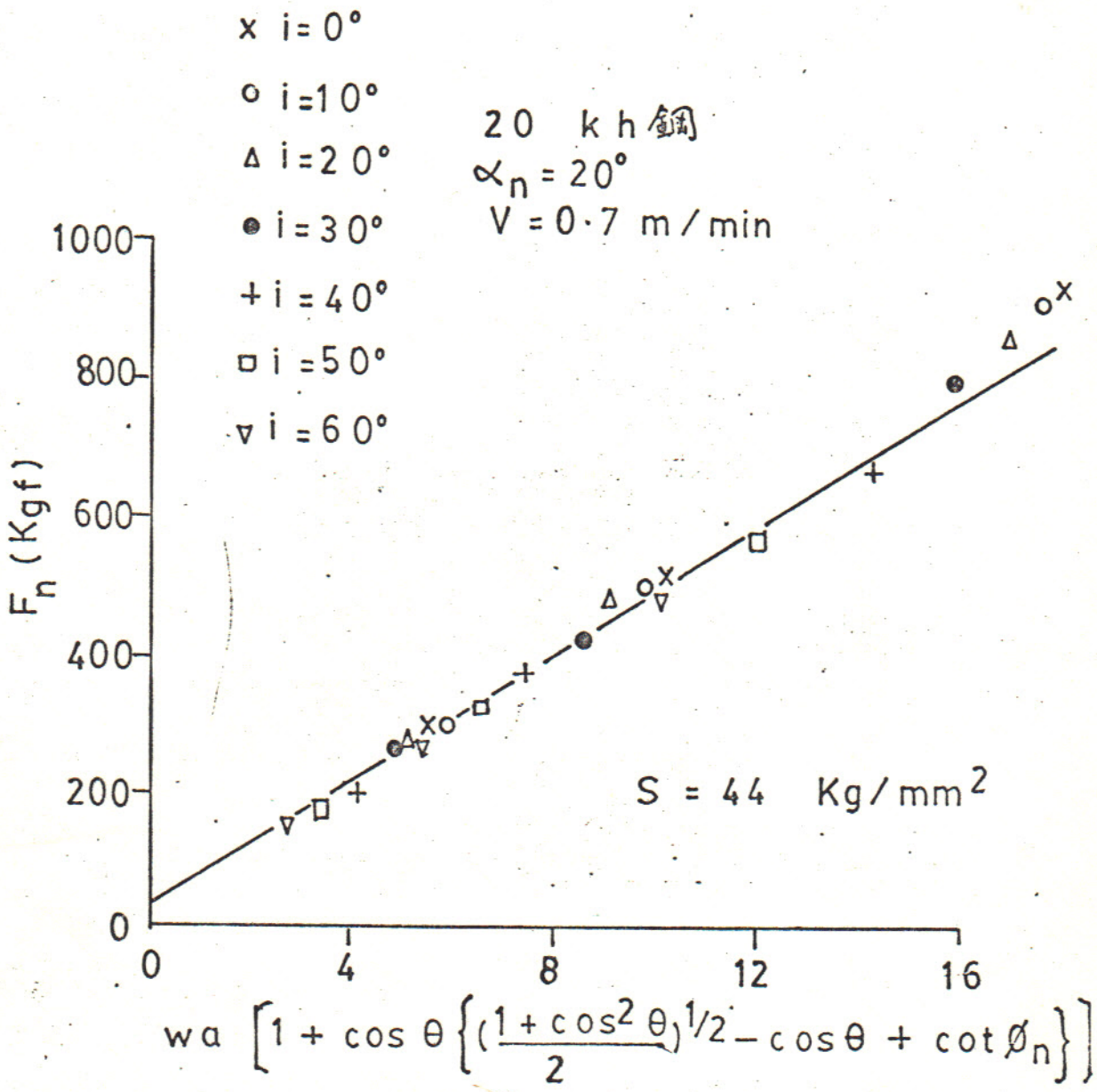

3.2 公式 (3.7) 的 S 值 (資料從 [25] 所得)

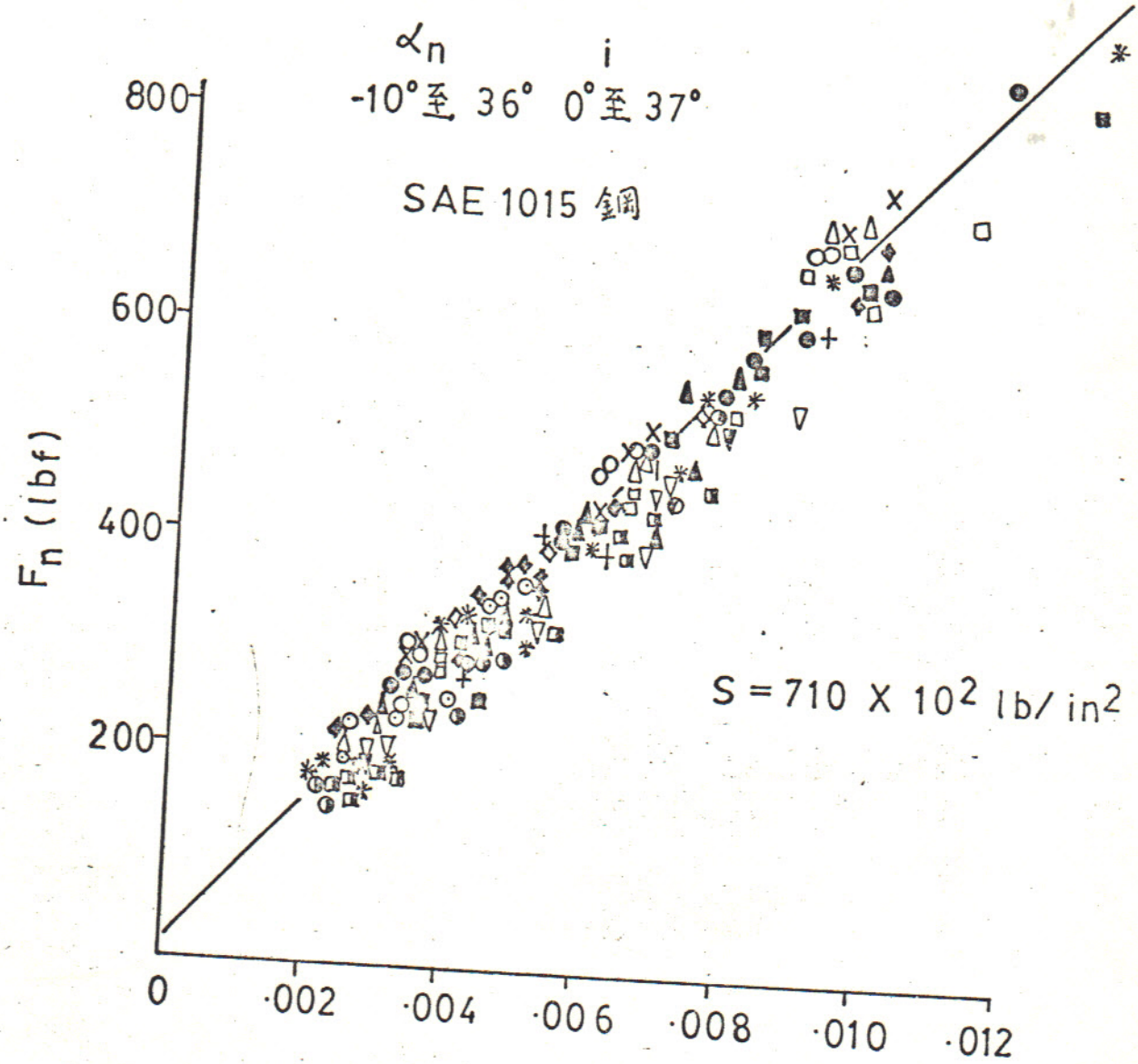

3.3 公式 (3.7) 的 S 值 (資料從 [26] 所得)

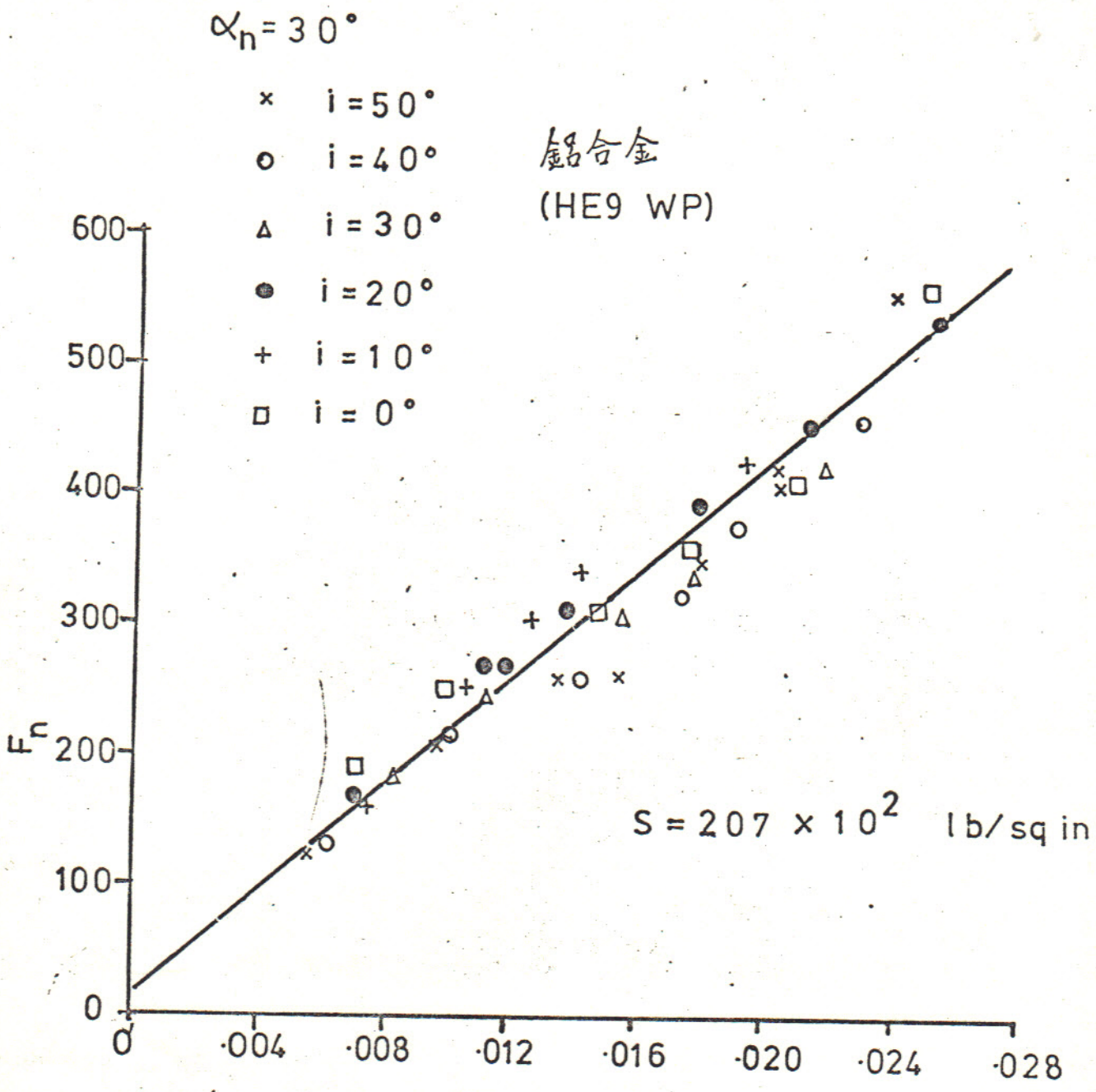

$$Wa\left[1+\cos\theta\left\{\left(\frac{1+\cos^2\theta}{2}\right)^{1/2}-\cos\theta+\cot\phi_n\right\}\right]$$

3.4 公式 (3.7) 的 S 值 (資料從 [27] 所得)

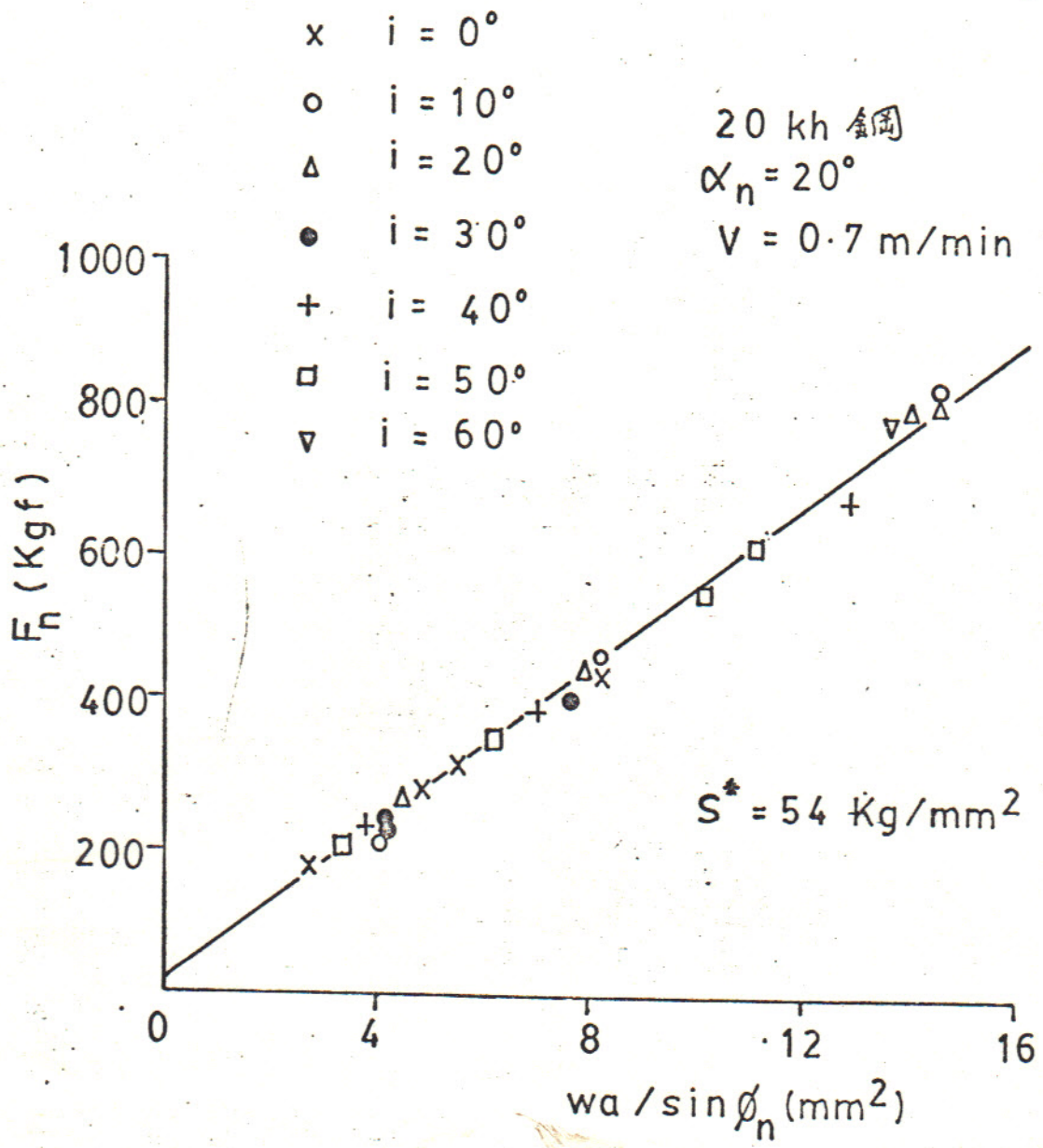

3.5 公式 (3.12) 的 S^* 值 (資料從 [25] 所得)

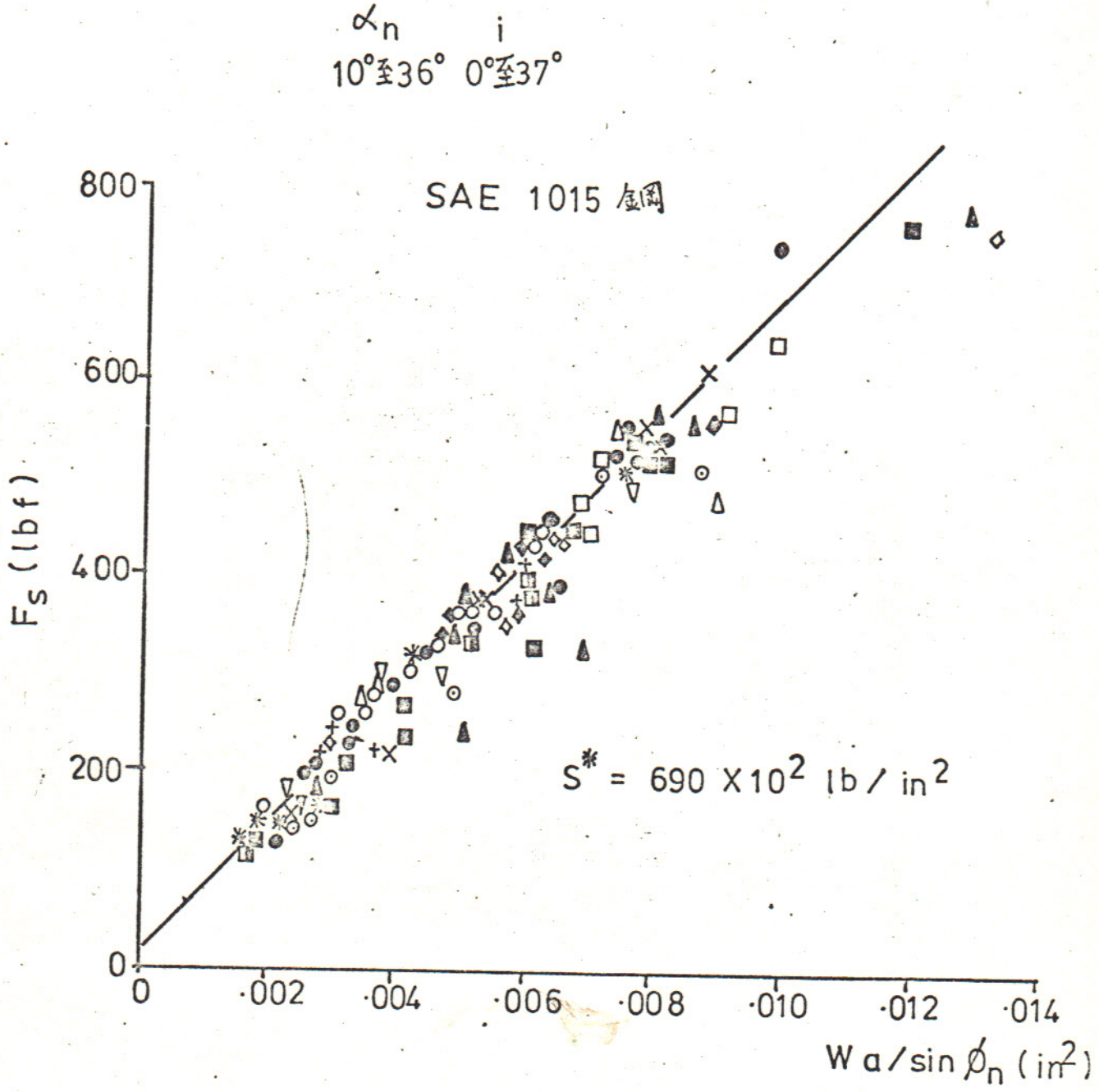

3.6 公式(3.12)的 S^* 值(資料從[26]所得)

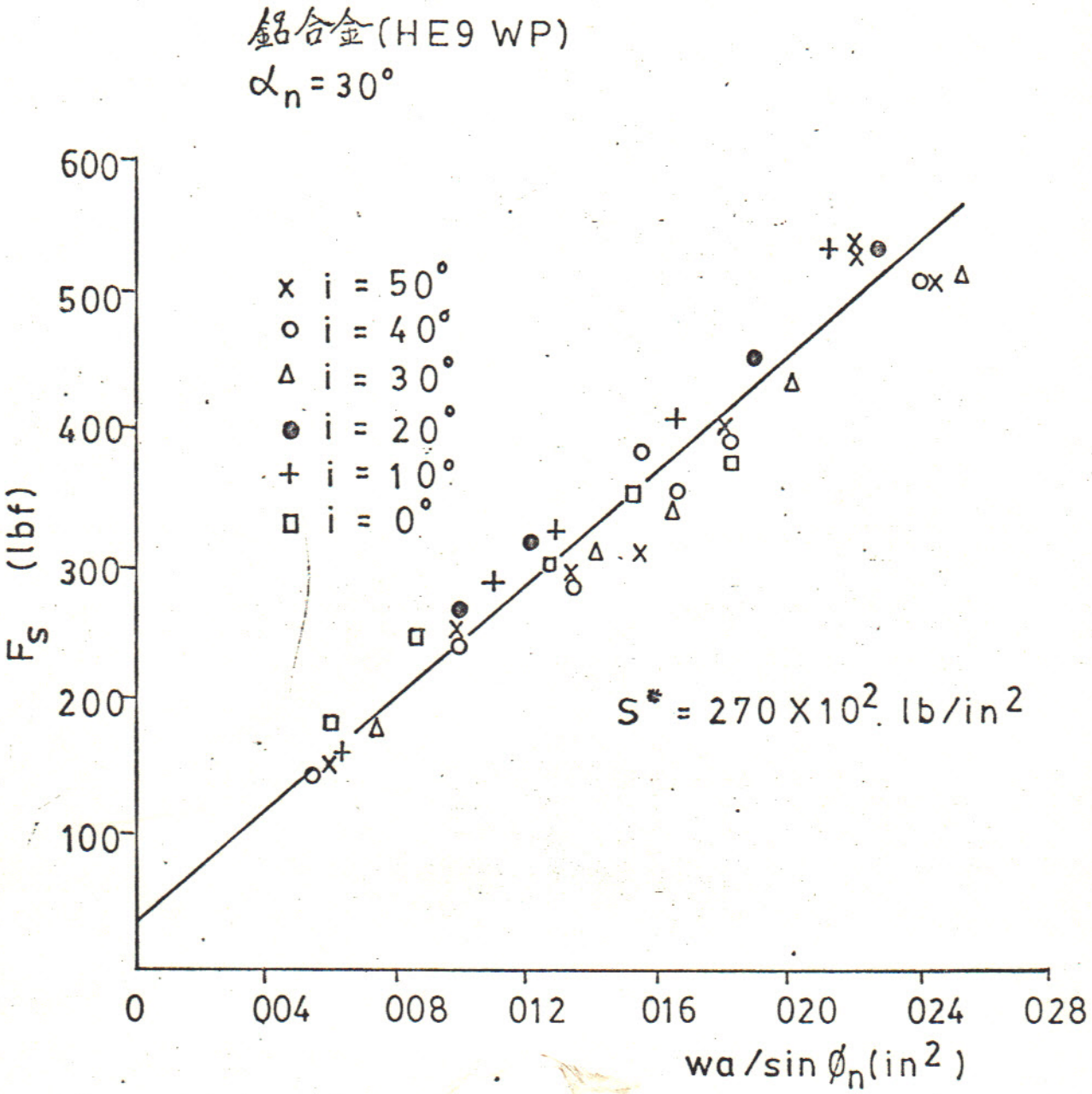

3.7 公式 (3.12) 的 S^* 值 (資料從[27]所得)

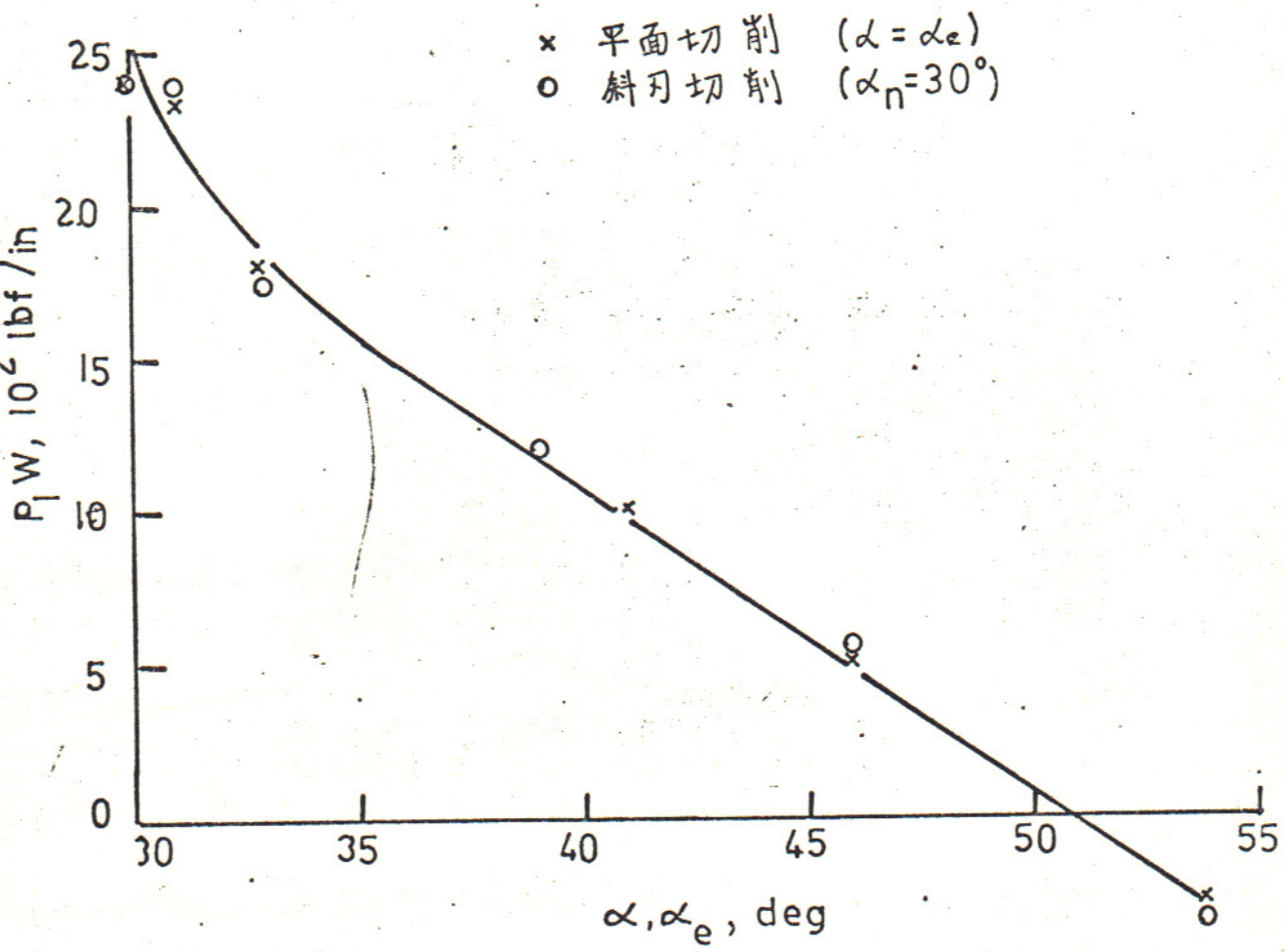

3.8 P_1W 斜刃切削與平面切削 ($\alpha = \alpha_e$) 的垂直压力比較

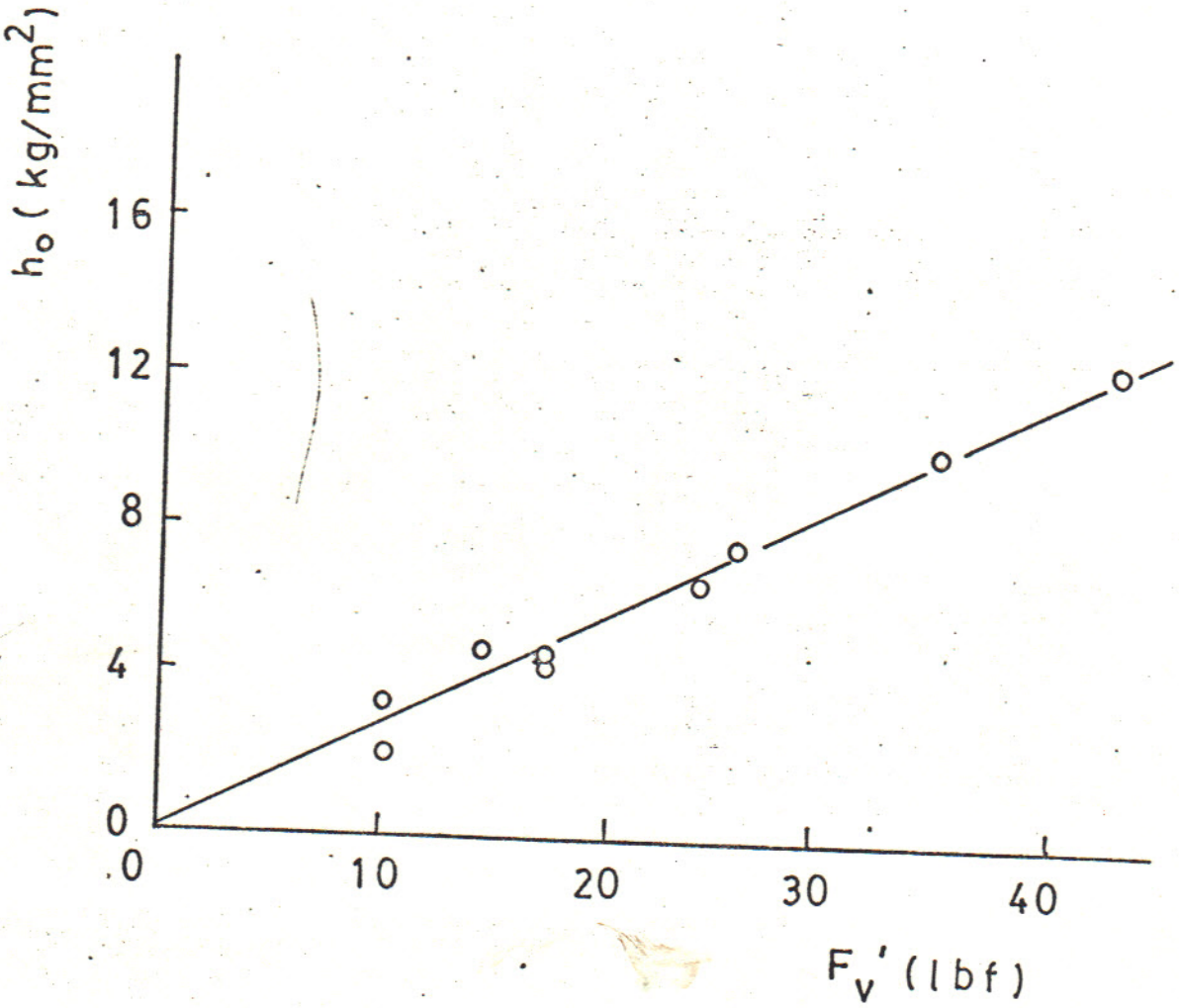

4.1 刃口圓弧半徑所引起的硬化 h_o 及垂直分向力 F_v' 的關係

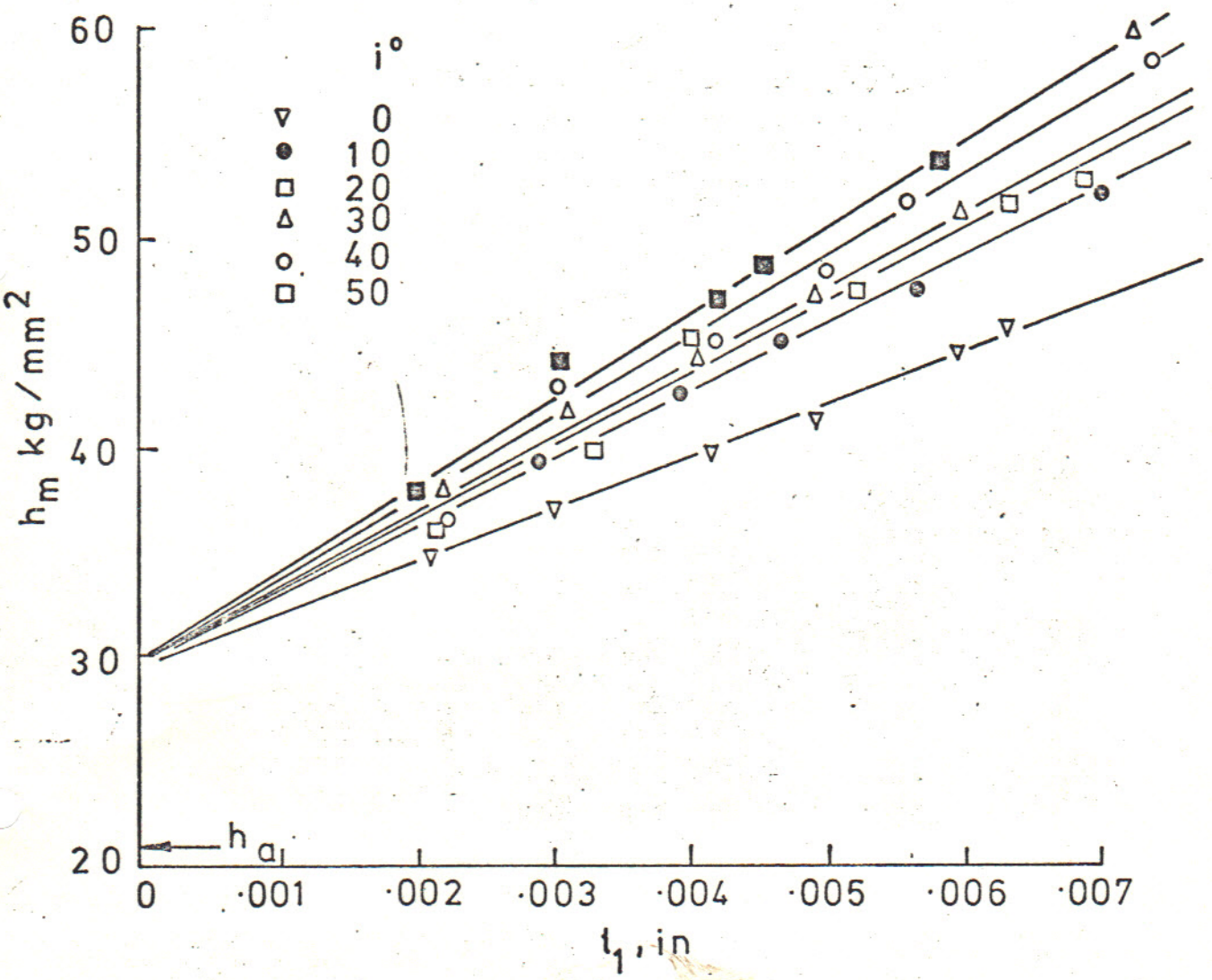

4.2 總表面硬化值与加工深度的関係

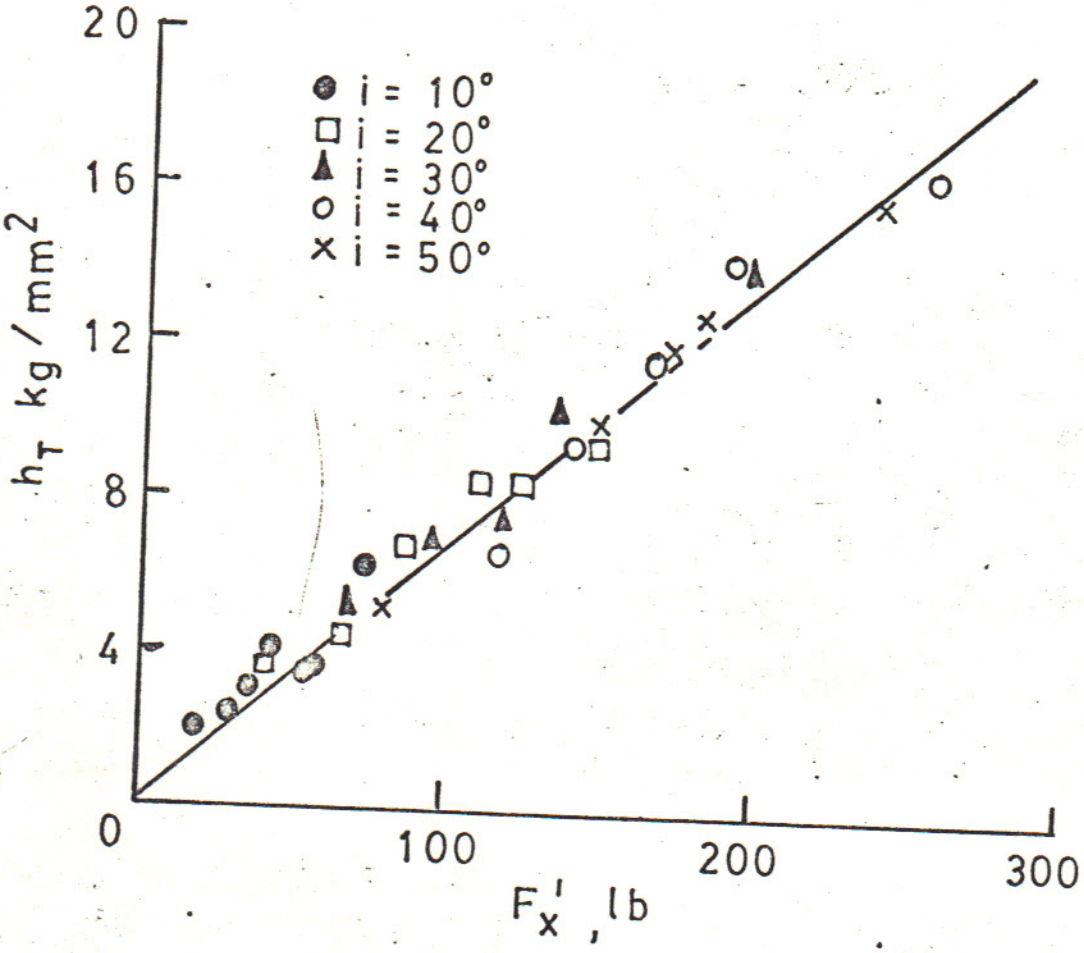

4.3 切削刃口圓弧半徑所引起的硬化 h_T 與切向分力 F_x' 的關係

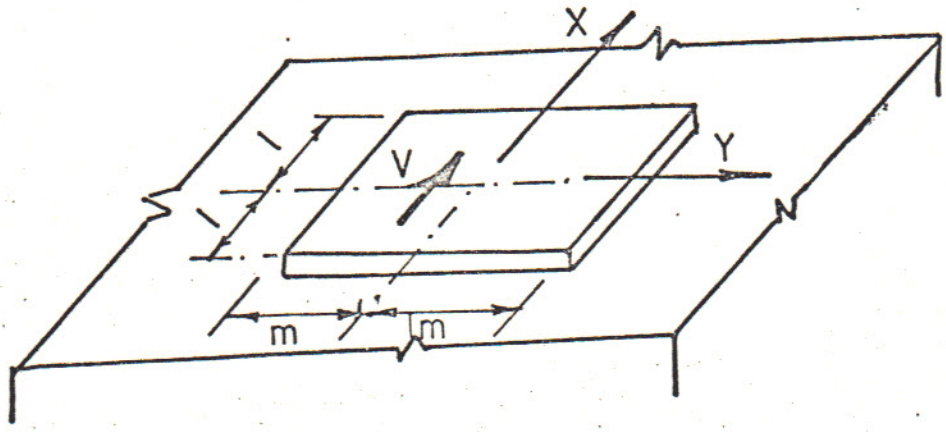

5.1 長形移動熱源示意图

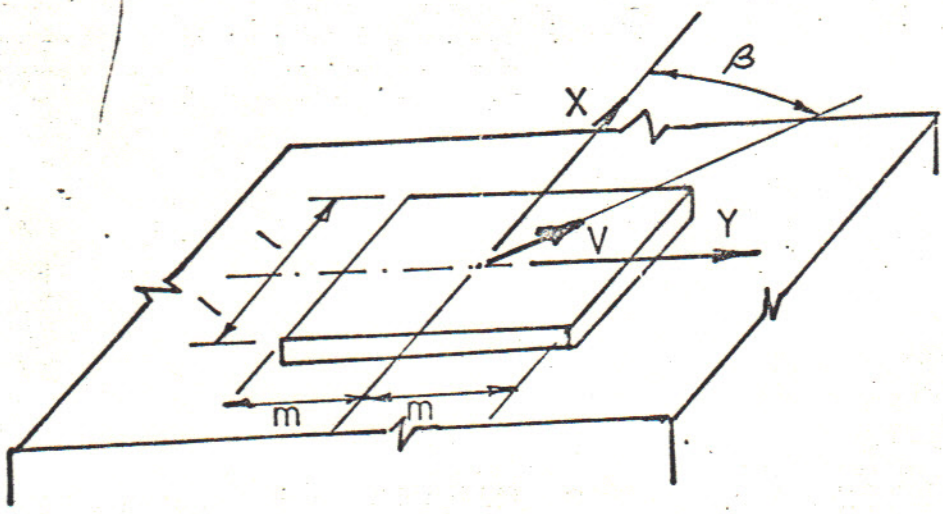

5.2 斜移熱源示意图

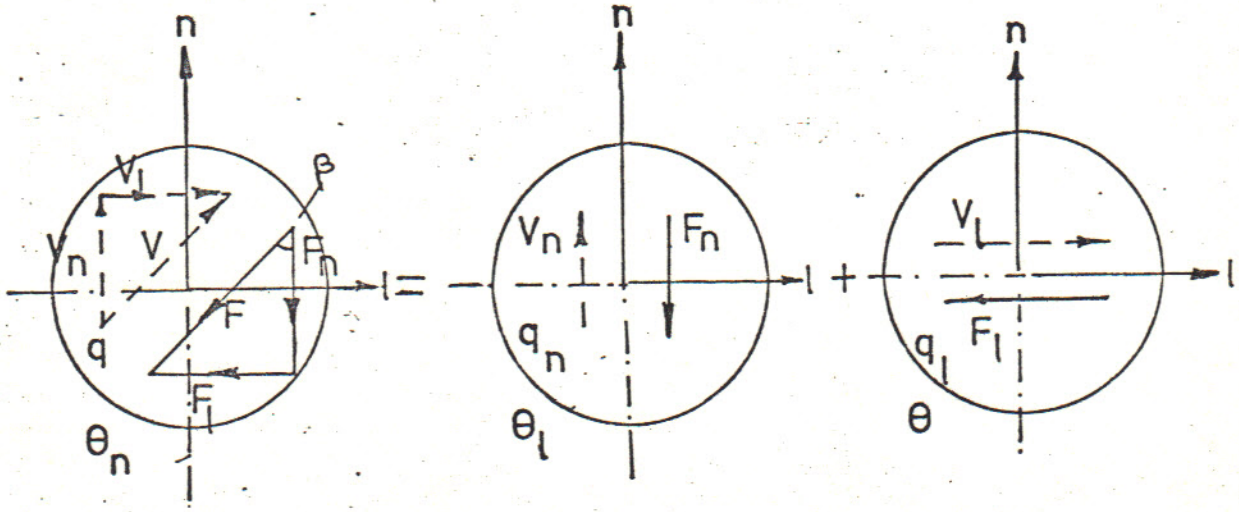

$$\theta = (\theta_n^{4/3} + \theta_l^{4/3})^{3/4}$$

5.3 斜放熱源的疊加原理

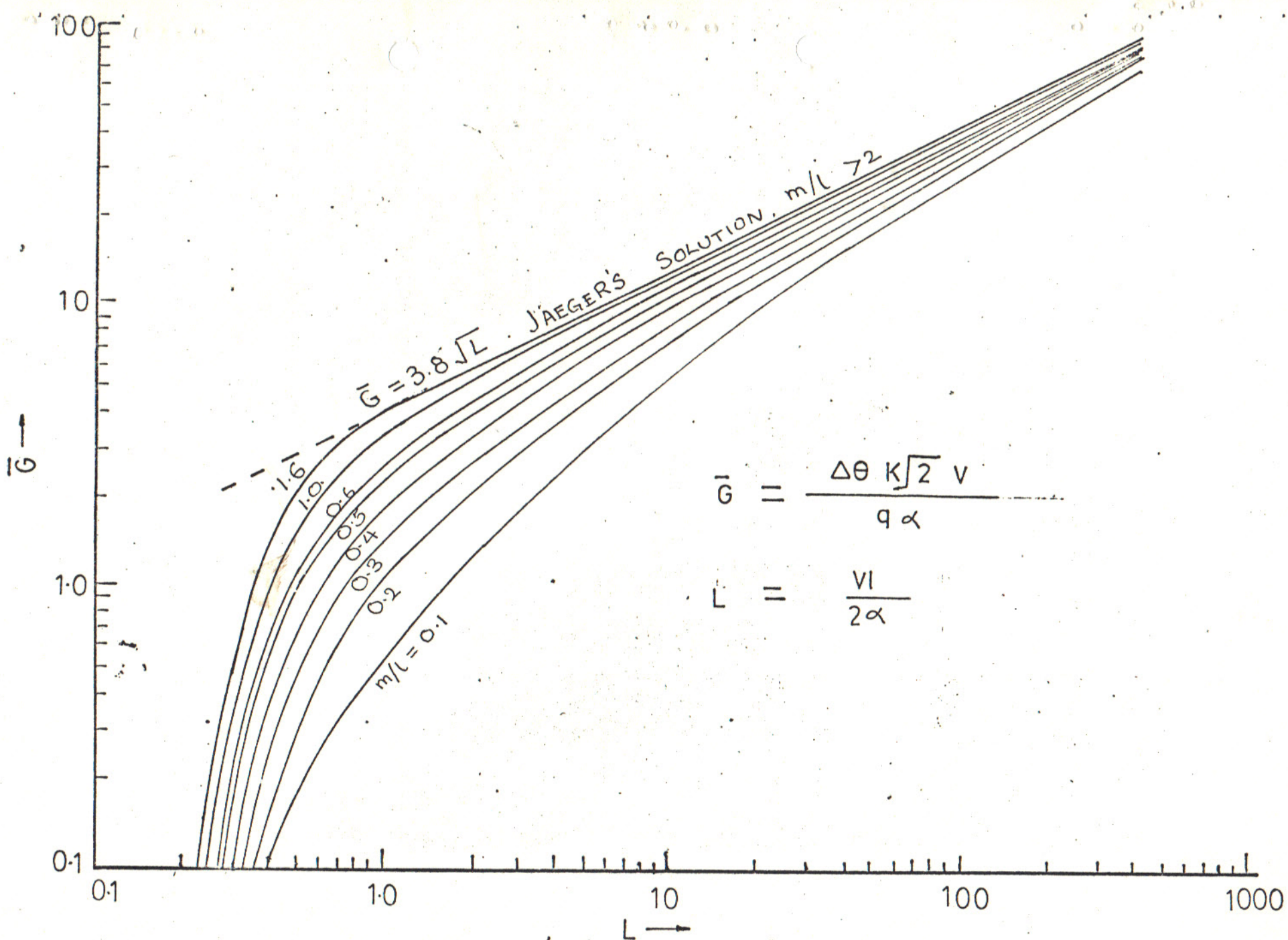

5.4 參數 $\bar{G}$ 的總表

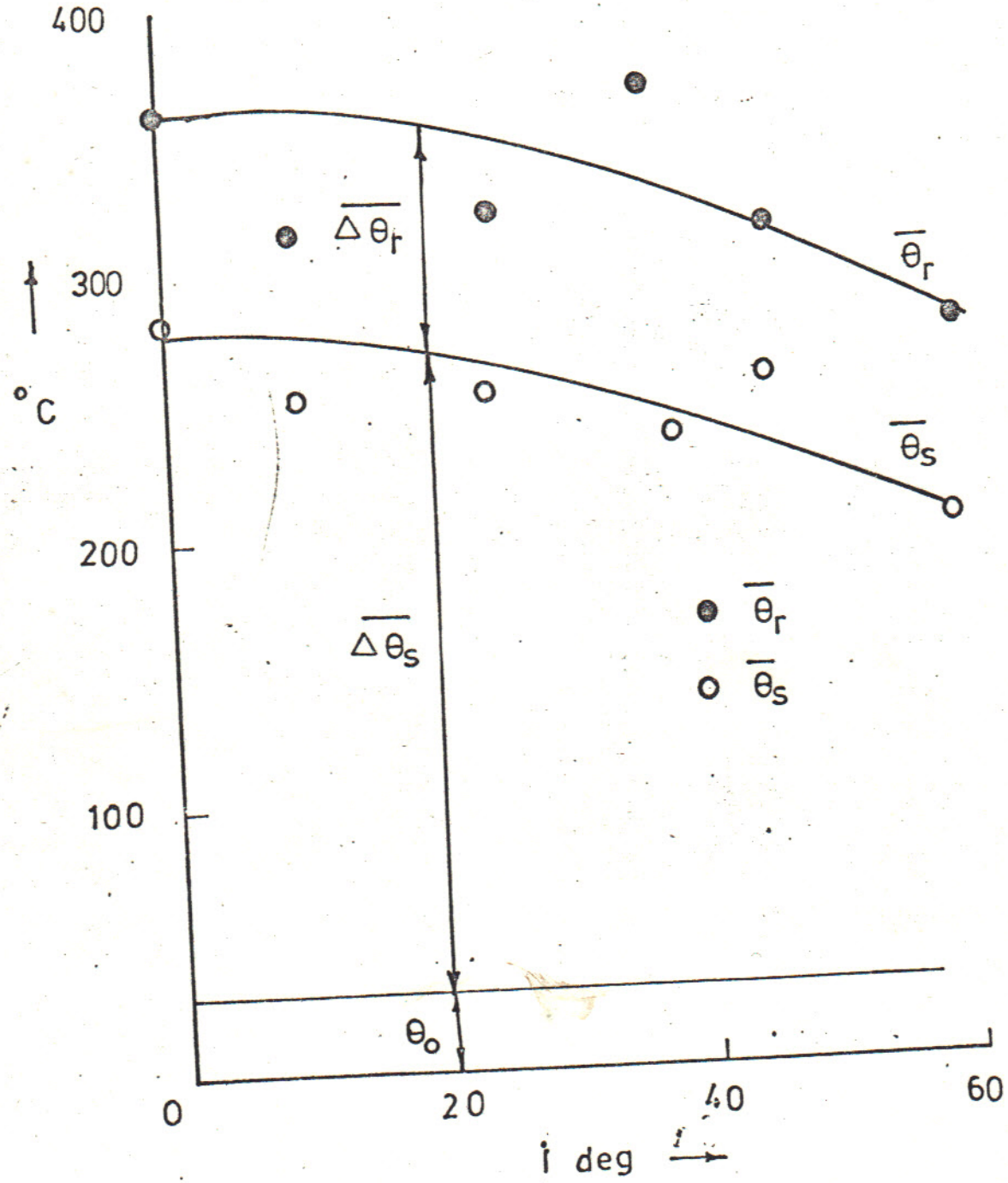

5.5 用疊加原理求出的溫度与斜角的関係

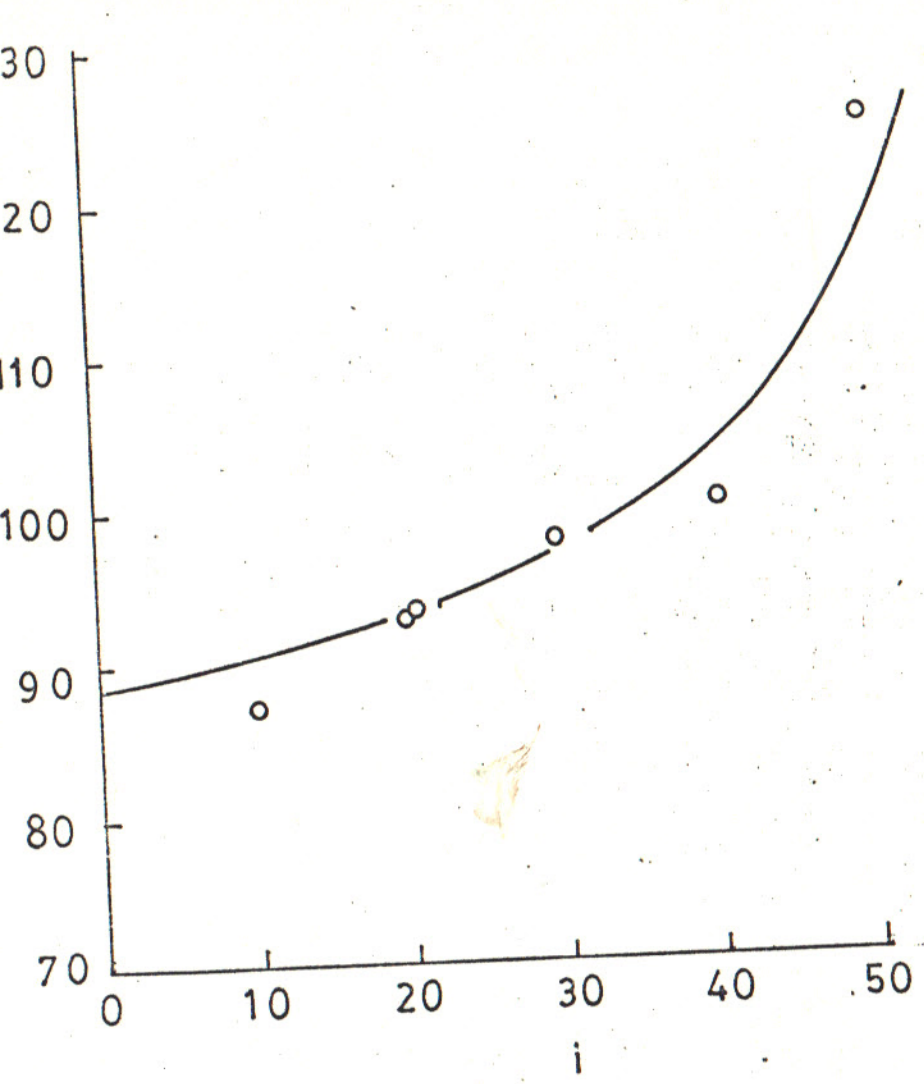

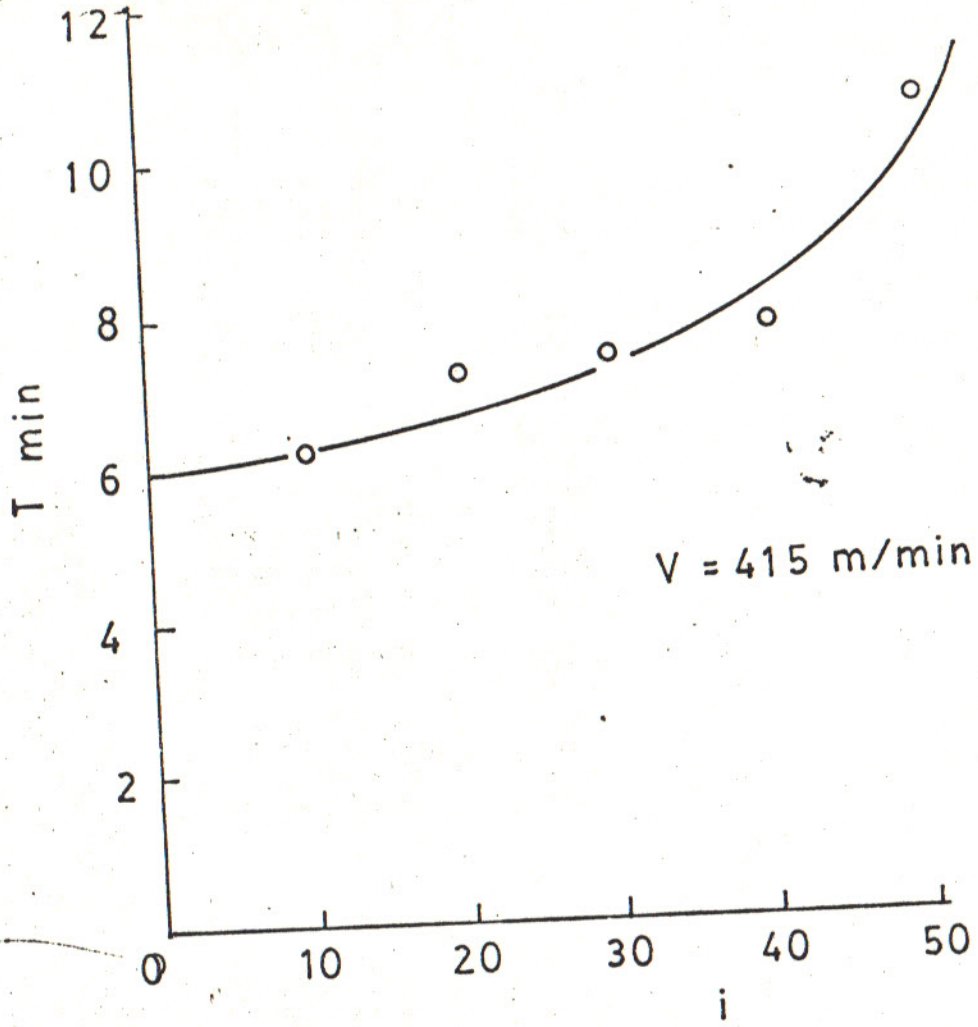

6.3 刀具斜角与刀具寿命及 C 的关系

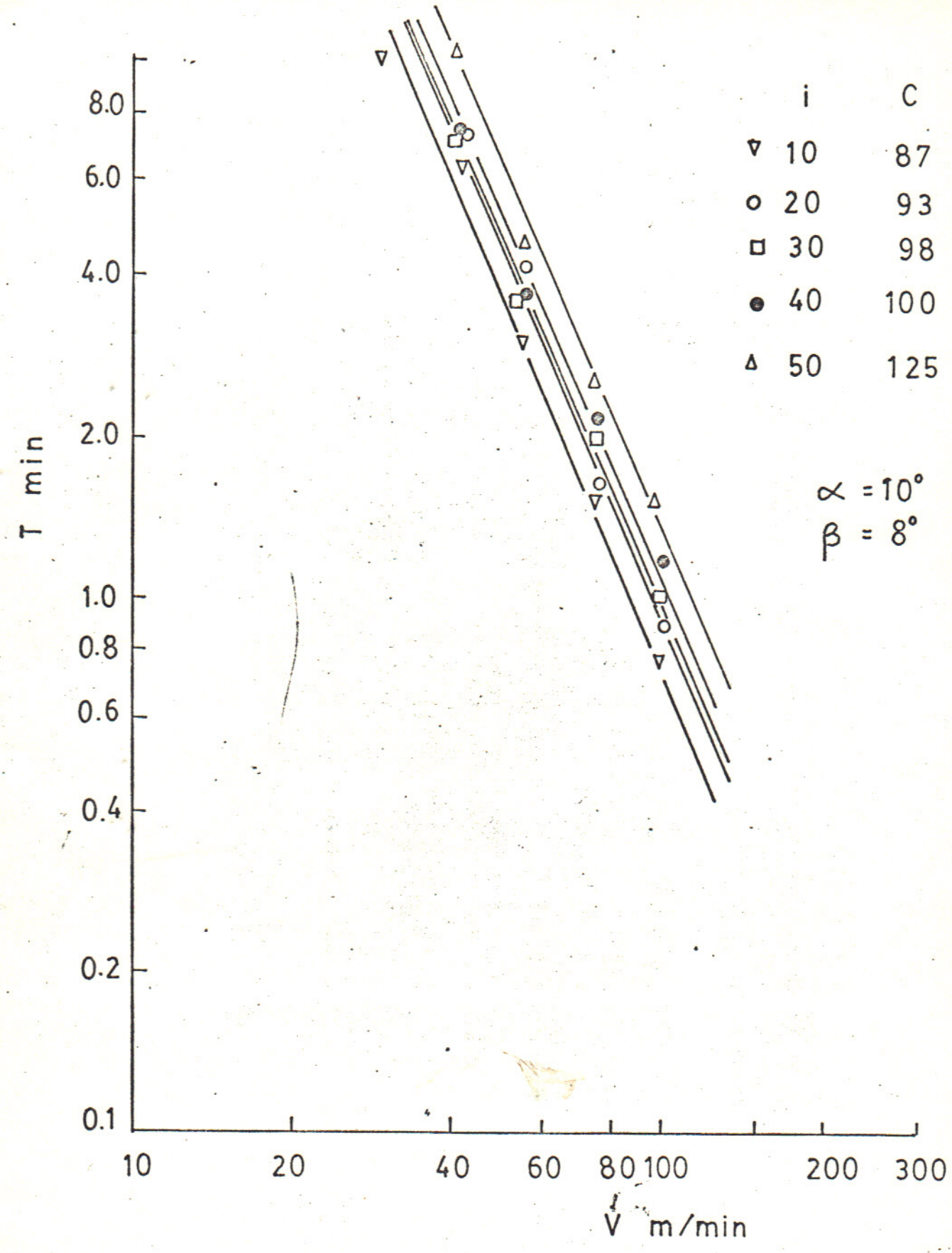

6.2 刀具壽命、速度与斜角的関係

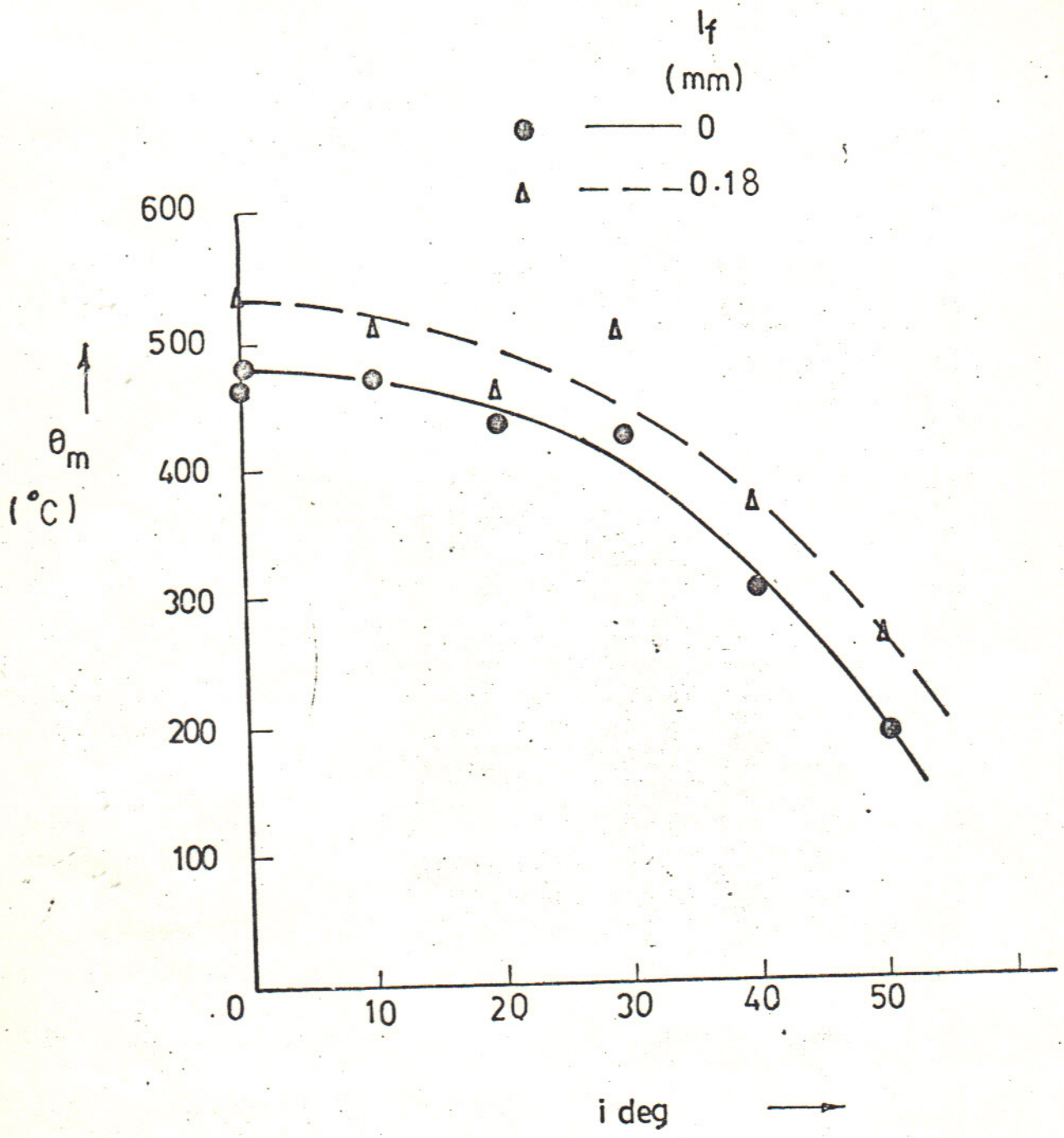

6.1 切削温度与斜角的实验关系